KERNFORSCHUNGSZENTRUM

KARLSRUHE

Oktober 1966

KFK 484

Institut für Experimentelle Kernphysik

Investigations on the Slotted Iris Structure

H. Eschelbacher

GESELLSCHAFT FÜR KERNFORSCHUNG M. B. H.

KARLSRUHE

KERNFORSCHUNGSZENTRUM KARLSRUHE

Oktober 1966 KFK 484

Institut für Exp.Kernphysik

Investigations on the Slotted Iris Structure

H. Eschelbacher

GESELLSCHAFT FÜR KERNFORSCHUNG M.B.H. KARLSRUHE

Investigations on the Slotted Iris Structure

H. Eschelbacher
Institut für Experimentelle Kernphysik der Technischen Hochschule und des Kernforschungszentrums Karlsruhe

I. Introduction

The slotted iris structure has been proposed and investigated by Giordano[1] for use in proton linear accelerators. Extensive measurements on this structure had been recently performed, so that we have gained a rather good survey on the behaviour of the slotted iris structure under geometrical variations[2]. From these measurements we hope to work out a useful theory in order to begin with computer calculations, especially for optimalization of the effective shunt impedance.

The models are built in the original size and investigated at room temperature not taking into account how to make the structure superconducting, which will be the final state of our work.

The first section of this paper reports the experimental optimalization of the slotted iris structure. We looked for the best shunt impedance with respect to geometrical parameters in a wide range of $\beta = v/c$, from $\beta = 0.35$ to $\beta = 0.90$. The second part reports on the investigation of special geometries of the coupling slots. It will be shown, that the coupling coefficient is strongly dependent on the slot angle, substantially more than on the slot width.

In the last section measurements of field distributions in the slotted iris structure will be given and the coupling in of the rf-power will be discussed.

II. Experimental Optimalization of the Slotted Iris Structure

1. Design of the Model

The slotted iris structure, which is shown in figure 1, was intended to operate at 760 Mc in the π-mode, because in the π-mode there is maximum shunt impedance. In a cylindrical waveguide the dominant mode with axial electric field is the TM010 mode. The boundary conditions give the lowest eigenvalue:

$$k_1 = \frac{2\pi}{\lambda_1} = \frac{\omega_1}{c} = \frac{2.405}{D/2} \qquad (1)$$

with D = diameter of the cavity.
This is only valid for a non-coupled isolated cavity. Since the cavities in the structure (i.e. a chain of coupled cells) are strongly coupled by the magnetic field, penetrating trough the slots, which are cut in the walls between adjacent cells, the π-mode frequency $f_{(\pi)}$ is lower than the 0-mode frequency $f_{(0)}$.[3,4]
The resonance frequency $f_{(n)}$ of the n-th mode is given by

$$\frac{f^2(n)}{f^2(0)} = \frac{1}{1 + K(1 - \cos k_n L)} \qquad (2)$$

$$k_n L = \frac{n\pi}{N} \quad (n = 0, 1, 2, \cdots, N) - \text{mode}$$

with k = coupling coefficient and N = total number of cells of equal length L in the structure.
For the π-mode (n=N) the phase shift between adjacent cells is kL = π and

$$\frac{f^2(\pi)}{f^2(0)} = \frac{1}{1 + 2K} \qquad (3)$$

The coupling coefficient K is then given experimentally by the width of the dispersion curve.
The resonance frequency of the unperturbed, non-coupled isolated cavity was chosen to be f_1 = 800 Mc, then a cavity diameter of

D = 288 mm results from equation (1). Without any drift tubes (see Fig. 3, l=0) the 0-mode frequency $f_{(0)}$= 800 Mc is just identical to the frequency f_1 of the non-coupled isolated cavity for all investigated slot widths. That means coupling is zero in the 0-mode and the 0-mode frequency is given by Eq. (1).

$$f(0) = f_1 = \frac{2.405 \cdot c}{D/2} \tag{4}$$

The second important parameter in the design of the structure has to be chosen in such a way that synchronism between the velocity of the particles to be accelerated and the phase velocity of the rf-wave is obtained.

$$\beta \lambda_0 = \lambda_g \tag{5}$$

with $\beta = v/c$, λ_0 = vacuum wavelength corresponding to $f_{(\pi)}$, λ_g = wavelength in the guide. Thus for the π-mode (n=N) we obtain the condition

$$\beta \lambda_0 = 2L \tag{6}$$

2. Variation of Geometrical Parameters

The influence of geometrical parameters was investigated for three different cell lengths:

L_1 = 98.8 mm (ß=0.5) corresponding to 145 MeV proton energy
L_2 = 135.0 mm (ß=0.7) " " 370 MeV " "
L_3 = 178.0 mm (ß=0.9) " " 1200 MeV " "

The cavity and drift tube diameters were kept constant for all measurements (D = 288 mm, d = 65 mm and beam hole diam. = 17.5mm). The length of the drift tubes was varied from a minimum value l=0 to a maximum l=117.2 mm. Slot width (SW) and slot angle (SB) were changed according to the numbers given in table I (see also Fig. 1).

SB	SW (mm)		SB	SW
49°	10 30 40 50 82	const. r_2=115 mm	57° 65° 73°	40 40 40
	66 108	const. r_2=141 mm		

Table I

The following measurements were performed with models consisting of three or six cells, respectively.

a) resonance frequencies for all modes
b) Q-values for all modes
c) effective shunt impedance for the π-mode

The coupling coefficient was calculated by equation (3) from the measurements of frequency.

3. Experimental Arrangement

We used a crystal controlled rf-generator (accuracy 10^{-8}) and a microampere meter to indicate the resonance maximum. The experimental set-up is shown in Fig. 2. For all measurements the position of the coupling loop feeding rf-power (20 mW) into the structure was fixed. Very loose coupling was arranged in order to have minimum perturbation by the loops. Thus the ratio 1/SWR was constant at a value of about 0.01 (SWR = Standing Wave Ratio).

a) Measurement of the Q-value

The measurements of the Q-value were based on the 3-dB method. The output voltage of the rf-generator (1V at 50Ω) was extremely stabilized and in addition to that controlled by a power meter. Since the coupling of power into the structure was quite

weak, the measured loaded Q_L was nearly identical with the unloaded Q_o . For this undercoupled case the following relation is valid.

$$Q_o = (1 + 1/SWR)\, Q_L \qquad (7)$$

Thus no correction of the directly measured Q-values was necessary. The accuracy of the Q-measurements was about $\pm$ 0.6 %. The Q-value of each geometry was measured three times and the average value had been taken. The reproducability was $\pm$ 1 %.

b) Measurement of the effective shunt impedance Z_{eff} $Z_{eff} = Z\, T^2$ (with T = Transit time factor) was measured according to the well known method introduced by Slater[5]. The experimental set-up is also shown in Fig. 2. The brass bead (Ø 8mm) and the Nylon thread (Ø 0.8mm) were the same for all measurements. Yet the error of the measured resonance frequency shift Δf is about $\pm$ 0.5 kHz, which corresponds to an error in the calculated Z_{eff}/Q of about 2.0 %. This is due to the uncertainty in finding the resonance maximum, because the Q-values are rather low in our demountable models, machined of brass. Measurements of the frequency deviation produced by the bead with a simple lock-in-oscillator were not successful, because no correct rf-phase properties could be achieved. Thus the shunt impedance infered from those measurements is about 25 % too low.

The coupling coefficient K derived from Eq. (3) can casily be determined experimentally.

$$K = (f_{\pi o}^2 - f_{\pi}^2)/2 f_{\pi}^2 \qquad (8)$$

From other approximative considerations follows, that K is proportional to the ratio of energy which contributes coupling, to the whole stored rf-energy in the cavity. This will be discussed later.

d) Scaling procedure

In order to have at a given frequency comparable figures of Q and Z_{eff}/Q scaling is necessary, because each geometrical variation of the cell, for instance drift tube length, cell length or slot size results in a shift of the resonance frequency of the mode. The directly measured Q-values were scaled to 760 Mc by multiplying by the square root of $(f_\pi/760)$. In addition they are multiplied by a factor of two, due to the different conductivity of brass and copper.

In order to find the optimum shunt impedance with respect to the drift tube length, the drift tube length is varied in several stops at constant cell length L. Thus the frequency is varied, resulting in different values of ß (Eq. 6). On the other hand all tanks of the linac should be excited with only one excitation frequency. In order to bring the frequency of each cell to the same value we could have changed some other geometrical parameters simultaneously, for instance the cell length or the cell diameter. We did not do this experimentally, but deduced it from the experimental results utilizing the frequency dependence of the parameters. Thus, it seems to be useful to interprete this variation of frequency as different values of ß.

The measured shunt impedance Z_{eff}/Q was scaled by a factor of $760/f_\pi$. In the normal conducting state Z_{eff}/Q is proportional to f and Z_{eff} is proportional to $f^{1/2}$.

4. Experimental Results

All experimental results are shown in the following figures. Figure 3 shows the measured dispersion curve for a structure consisting of 3 cells (2 half cells at each end) for different drift tube lengths and slot widths. The calculation of the dispersion curves according to Eq. 2 is in very good agreement with the measurements. The mean deviation is only 0.2 %. Fig. 4 and Fig. 5 give the resonance frequencies of the π-mode versus ß, measured with models having a constant slot angle of SB = 49°

and the two slot widths of SW = 82 mm and SW = 40 mm, respectively. These figures were taken at three different cell lengths L_1, L_2 and L_3 . Parameter is the drift tube length which is varied from l=0 to l=117.2 mm. Each measured frequency f_π corresponds to one value of $\beta = 2Lf_\pi/c$. The three straight lines include all points with constant cell length.

The frequency of the π-mode (all other modes are treated in the same way) is strongly decreased by increasing the drift tube length, because the drift tubes represent a considerable perturbation with respect to an unloaded cavity. Fig. 8 shows the π-mode frequencies versus slot width at a constant slot angle of SB = 49° for a certain number of investigated drift tubes and all lengths. Fig. 9 continues Fig. 8 down to lower frequencies. The minima of the π-mode frequencies point out the maxima of the coupling coefficient K.

The measured Q-values of the π-mode are shown in Fig. 10, which gives a comparison between the two slot widths at the same slot angle versus ß. The points clustering in three regions of the diagram correspond to the measurements at the three cell lengths, each with a set of different drift tubes. As expected the Q-values of the 0-mode are higher than those of the π-mode by an average factor of about 1.62 . Due to the maximum current flowing on the disks of each cell, the π-mode is the mode with the lowest Q-value. Fig. 10 shows, that for ß greater than about 0.6 the Q-value of a structure with a slot width of SW = 82 mm becomes significantly higher than for SW = 40 mm .
This effect can be understood by an investigation of the coupling through the slots from cell to cell. The coupling coefficient K describes the strength of coupling and depends more or less sensitively on the geometrical variations of the cell, since the energies participating in the coupling are influenced. From the measurements of the resonance frequencies of the modes, K is calculated (Eq. 8) and plotted in Fig. 11 and Fig. 12 for SW = 82 mm and SW = 40 mm, for a constant slot angle of SB = 49°. Both figures show the decrease of K with increasing ß, i.e.

increasing cell length at constant frequency. This can be seen obviously in Fig. 13 . Comparing these effects with Fig. 10 we conclude, that intensive coupling lowers the Q-value. The results of these measurements shown in Fig. 14 prove this assumption. In other words, if the coupling is increased Q becomes lower. For all values of ß greater than 0.6 case of SW = 40 mm (Fig. 12) the coefficient K is remarkable higher than for SW = 82 mm (Fig. 11) .

Strong coupling is generally achieved by enlarging the slot in the region of strong magnetic fields. This causes a considerable lengthening of the current paths on the disk, so that more dissipation occurs. In Fig. 15 this effect is shown. The slot angle has been increased in several steps at a constant slotwidth of SW = 40 mm. The coupling coefficient becomes nearly 40 % at a slot angle of SB = 73°, in comparison to 10 % at a slot angle of SB = 49°. The more the effective azimuthally length of the slot reaches the value of half a wavelength, pure resonant coupling will be approached. Then theoretically K tends to infinity. Additional effects concerning K occur by the influence of drift tubes and slotwidth. The clear minima of π-mode frequency at SW = 40 mm in Fig. 8 point out the maxima of K, which can be seen in Fig. 16. In order to check the limiting case without slots (SW = 0), only disk with a center hole of the same diameter of the beam aperture in the drift tubes (17.5 mm Ø) were investigated. By this way the structure was changed into a normal iris structure with a very low coupling coefficient of K = - 0 . 16 % .
Measurements with a center bore hole of 40 mm diameter gave a value of K = - 0.31 % .
These results demonstrate the following:
The coefficient K may be defined by the fraction of the energy participating in the coupling (i.e. coupling energy W_K), to the total stored energy within the cell (i.e. W_S).

$$K \sim W_K / W_S \qquad (9)$$

On the other hand the coupling energy W_K can be described by the square of the deflected current flowing around the slot multiplied

by the effective impedance Z_S of the slot.

$$W = \text{const} \cdot J \cdot Z_S \qquad (10)$$

The characteristic impedance can be determined experimentally in a electrolytic tank. Current and effective impedance are dependent on slot dimensions and geometrical parameters, which describe where the slot is located on the disk. If the slot angle is increased more current is deflected by the slot and J becomes high. The reduction of coupling with increasing ß, i.e. longer cell length (Fig. 13), is due to the increase of total stored energy , while the coupling energy remains constant, because no other parameters were varied (Fig. 11 and 12). Considering a cavity without drift tubes (l = 0), maximum coupling occurs at the slot width SW = 40 mm, because only the magnetic field energy contributes to the coupling energy. On the other hand the coupling is less at a slot width of SW = 82 mm, since the electric field energy participates in the coupling energy. The influence of the electric field in the coupling region is opposite to the magnetic field and produces a raise of π-mode frequency, thus the coupling will be reduced. Drift tubes cause a concentration of the axial electric field in the middle of the cell, but only a slight displacement of the magnetic field towards the middle of the cell. Thus with drift tubes the electric field is removed from the slots and becomes less effective in negative coupling. The influence of drift tubes on pure magnetic coupling, for instance in the case of slot width SW=40mm (see Fig. 13), is not large, since the magnetic field is much less perturbed in this way. From this dependence of the coupling coefficient and from the connection between K and Q some statements may be made concerning the effective shunt impedance. It will be expected that structures with strong coupling have lower shunt impedances, because Z_{eff} is directly proportional to the Q-value. The results of measurements are summarized in the following figures.

Fig. 17 and Fig. 18 show the values of Z_{eff} versus ß (as deduced from the bead measurements of Z_{eff}/Q and the measurements of Q) for different cell lengths and a slot width of SW = 82 mm and SW = 40 mm, respectively. Z_{eff}/Q and Q are scaled to 760 Mc. The values of ß are calculated from the cell length and the directly measured frequency of the π-mode belonging to a special geometry of the cells, as described in section 3d. The dotted lines connect those figures measured at the same cell length. At high ß the effective shunt impedance in the case of SW = 82 mm is better than for SW = 40 mm, due to the good Q-values (i.e. low coupling). The shunt impedance increases with ß, since the coupling drops with ß. This is given in Fig. 19 and Fig. 20, where Z_{eff} is plotted versus K. The final results of shunt impedance with respect to the drift tube length are given respectively. Lines of constant ß, extending from ß = 0.35 to ß = 0.9 are depicted from Fig. 17 and 18. Along these curves of constant ß each point corresponds to a different cell length and therefore to a different frequency. But we need lines of constant frequency, which we may obtain from the frequency plotted versus ß (Fig. 4 and 5), by drawing lines at constant frequencies and interpolating the associated drift tube length [1]. Then the lines with constant frequency are fixed by the cross-points of lines with constant ß and the interpolated value of l. At ß smaller than about 0.7 a maximum of the effective shunt impedance occurs at drift tube lengths between l = 60 mm and l = 75 mm. A similar maximum at higher values of ß could not be measured, since only drift tubes up to a length of l = 96.2 mm had been investigated. Some uncertainties may possibly exist in this region, but probably such maxima will occur. At nearly all figures of ß the curves of constant frequency run trough those maxima. From these curves we conclude that for both slot widths the investigated model, which had a diameter of 288 mm, ougth to be excited with a frequency of about 650 Mc, if one desires to operate at maximum shunt impedance for all values of ß.

The optimal slotted iris structure

Finally the optimal geometrical dimensions with the frequency of 760 Mc are obtained by linear scaling of all geometrical parameters

with a factor of 650/760. Then the curves of constant frequency become also curves of constant tank diameter. Thus the measurements lead to the following optimal structures for a constant slot angle of SB = 49°, which are listed in table II, for an operating frequency in π-mode of 760 Mc. The results are plotted in Fig. 23 . The structure with a slot width of 82 mm is to be prefered.

		SW = 82 mm		SW = 40 mm	
ß	l [mm]	l [mm]	$Z_{eff}[\frac{M\Omega}{m}]$	l [mm]	$Z_{eff}[\frac{M\Omega}{m}]$
0.35	69,1	51,3	17,2	36,3	15,6
0.50	98,8	53,9	17,5	52,2	17,2
0.55	108,6	55,2	17,7	--	--
0.60	118,4	56,9	18,1	57,3	18,1
0.65	128,3	59,0	18,8	60,7	18,8
0.70	138,2	62,0	19,8	64,1	19,7
0.75	148,1	65,0	21,5	66,7	21,3
0.80	157,9	67,1	23,5	68,4	23,0
0.85	167,8	69,7	26,7	--	--
0.90	177,6	71,8	30,3	69,7	24,6

tank diameter: 246,3 mm
drift tube diameter: 55,6 mm
beam aperture: 15,0 mm

Table II

Measurements with drift tubes with the same outer diameter of d = 65 mm but a larger beam hole of 30 mm in diameter yield lower values of shunt impedance, as expected.

III. Investigations of Different Geometries of Coupling slots

In the following investigations will particularly be reported about the influence of slot angle and slot width on frequency, coupling coefficient K and Z_{eff} . All these measurements were performed with but one cell length of L = 98.8 mm.

The resonance frequency of the π-mode rapidly decreases linearly by increasing the slot angle at constant slot width of SW = 40 mm. Both effects, increasing the slot angle and reducing the drift tube length give a practicable method of tuning the cells to the same frequency. The coupling coefficient is steeply raised up to 37 % at a slot angle of SB = 73° (Fig. 15). This points out that resonant coupling is nearly reached,because an effective azimuthally length of the slot is onlarged nearly to the order of half a wavelength. For all three cell lengths the coupling coefficient shows the same dependency on the slot angle, but in comparison to L_1 it is about 2.25 % lower at L_2 and 3.75 % lower at L_3. Structures with strong coupling of this kind seem to be not interesting, since they will give no optimal shunt impedances. Only when resonant coupling is obtained such structures will operate more successful.

Table I gave a summary of the investigated geometries of the slots. So far we discussed only the measurements performed with cells, where the slot width was fixed by the constant outer radius r_2 = 115 mm .

In the following the two most interesting slots (SW = 40 mm and SW = 82 mm) had been onlarged in slot width up to r_2 = 141 mm near to the outer radius of the cell which is R = 144 mm. The slot angle SB = 49°) and the inner radius of the slot was kept constant at r_1 = 75 mm and r_1 = 33 mm, respectively. Thus resulting to a slot width of SW = 66 mm and SW = 108 mm, respectively. Measurements were done with a cell length of 98.8 mm for all drift tube lengths. The results are shown in Fig. 24 for shunt impedance and in Fig. 25 for coupling coefficient. The

data of SW = 40 mm and SW = 82 mm have also been plotted, in order to give better comparison. To each point belongs a different frequency. The stronger coupling is due to the enlargement of the slot towards a region where the magnetic field dominantly contributes to the coupling energy. A small decrease of the shunt impedance occurs, as expected. In the case of SW = 82 mm and SW = 108 mm the drift tubes prevent the electric field to participate in coupling, thus K becomes larger with longer drift tubes. On the other hand, if maximum coupling has already been achieved at 1 = 0 (see Fig. 16) the drift tubes produce a slight shift of the magnetic field into the middle of the cell, away from the coupling slot.

For all slot geometries investigated so far, the vertex of the slot angle was fixed at the axis of the cell (i.e. the center of the beam hole). Considering that coupling is constitively influenced by the amount of the deflection of the current paths, slots as shown at the top of Fig. 26 seemed to be practicable. In contrast to SW = 82 mm the current paths are now straight radial lines and no deflection does occur at the transition of current from the drift tube to the disk. Thus the vertex of the slot angle is transposed to the outer diameter of the drift tube. We investigated two different geometries, both with a slot width of SW = 82mm (r_2 = 115 mm) and slot angles of SB = 65° and SB = 86°, respectively. The latter case is comparable with a structure where the drift tubes are supported by four nearly parallel bars. In addition to that we made an experiment with a configuration where the disk had been rotated from cell to cell by an angle of 45°, resulting in a special kind of cross-bar structure. The experiment results are shown in Fig. 26 and Fig. 27, all measured with a cell length of L = 98.8 mm. The coupling coefficient at a slot width of SW = 82 mm is linearly depending on the drift tube length. Incomparison to other slot shapes no improvement in shunt impedance can be observed.

Another experiment was performed with elliptical slots. The long axis of the ellipse with a length of 108 mm was in radial direction,

the length of the short axis was 40 mm. This attempt was not successful because the coupling between cells was too weak. Considering, that coupling is mainly given by the dimension of the slot angle (See Fig. 15), those slots are not effective.

IV. Measurement of Field Distribution of the π-mode in the Slotted Iris Structure

These measurements were executed according to Slater's method [6]. The electric field was measured with a pure dielectric bead ($BaTiO_3$), and the sum of electric and magnetic field by a metallic bead (brass). The cell length was 98,8 mm and the drift tube length l = 51 mm. The measuring equipment was the same as shown in Fig. 2 .

After calibrating the two beads, the electric field distribution may be evaluated qualitatively by using Slater's formula

$$\frac{\Delta f}{f} = \frac{3}{4} \cdot \frac{V}{W \cdot \varepsilon_0} \left(E^2 - \frac{1}{2} Z_0^2 H^2 \right) \tag{11}$$

with V = volume of the bead
W = stored energy in the cell
$\varepsilon_0 = 8.8594 \cdot 10^{-12}$ Asec/Vm
$Z_0 = 377$ = impedance of vacuum
f_0 = unperturbed resonance frequency of the μ-mode

From the measurement with the dielectric bead follows

$$E^2 = \frac{\Delta f_1}{f} \cdot \frac{4}{3} \cdot \frac{W}{V \cdot \varepsilon_0} \tag{12}$$

with f_1 = frequency shift produced by the dielectric bead.

In order to get a qualitative statement of the field distribution, the term $4W/3V \cdot \varepsilon_0$ may be set to unity, since the stored energy is not known exactly. The measurements with the metallic bead produce the frequency shift f_2 , then the magnetic field is given by

$$H^2 = \frac{4W}{3V \cdot \varepsilon_0} \cdot \frac{2}{Z_0^2} \left(\frac{\Delta f_1}{f_0} - \frac{\Delta f_2}{f_0} \right) \tag{13}$$

We measured the radial distribution of the fields at the two distinguished azimuthal positions, first over the slots and then over the remaining metallic sections of the disks. Seven measurements with both beads were performed at different positions within one cell. From these measurements we calculated the strength of the magnetic field near the outer radius along the length of the cell in order to find the position, where the coupling loop has to be located. The result is given in Fig. 30 and shows the magnetic field, which is seen by a coupling loop diving 15 mm into the cell when moving the loop parallel to the outer lining from one disk to the next. The loop area is perpendicular to the azimuthal component of the magnetic field. It can easily be seen, that the magnetic field between the slots (i.e. in front of the stems) is about twenty times higher than in the slot region. Thus, coupling power into the structure is most officient if the loop is located between two slots and somewhat outward the middle of the gap. In this position matching with the rf- generator will easily be achieved.

References

1) S. Giordano, Minutes of the 1964 Conference of Proton Linear Accelerators, MURA, 60, 1964

2) W. Bauer, H. Eschelbacher, M. Kuntze
Kernforschungszentrum Karlsruhe
KFK - Reports No 346 and No 403

3) T. Nishikawa, S. Giordano, D. Carter
The Review of Scientific Instruments
Vol. 37, No 5, 652, 1966

4) H. Eschelbacher, to be published

5. J.C. Slater, Microwave Electronics
D. Van Nostrand Comp., New York, 1963

6) L.C. Maier, J.C. Slater
Journ. Appl. Phys. 23, 1952

Fig. 1

Slotted Iris-Model

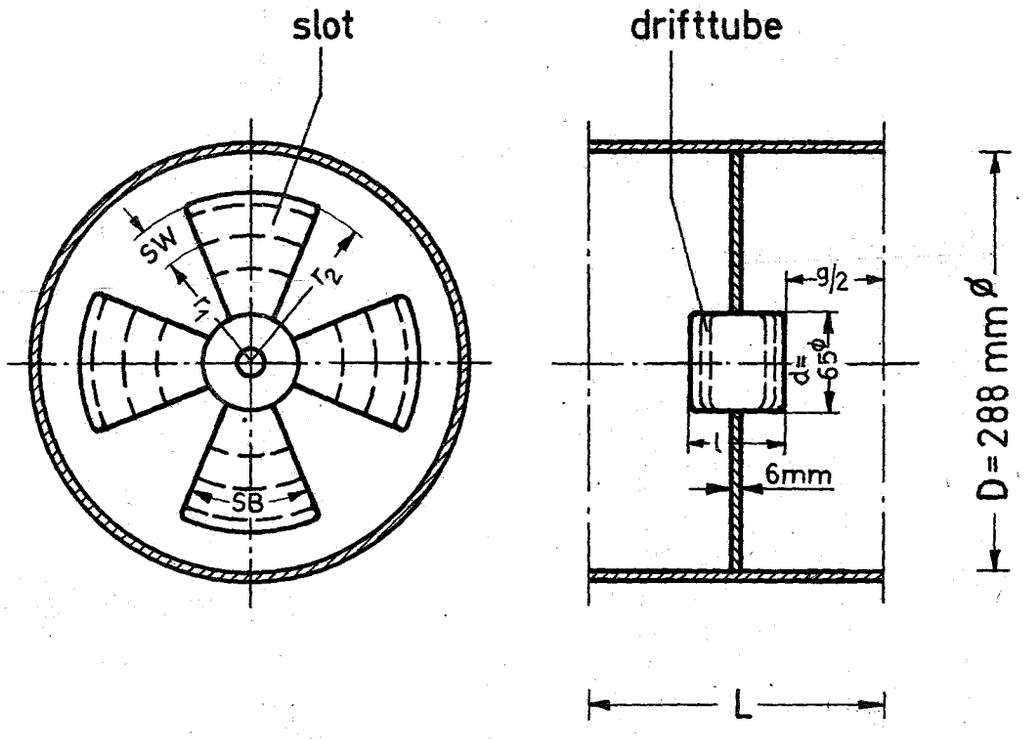

dotted lines show the variation of drifttube length and slotwidth

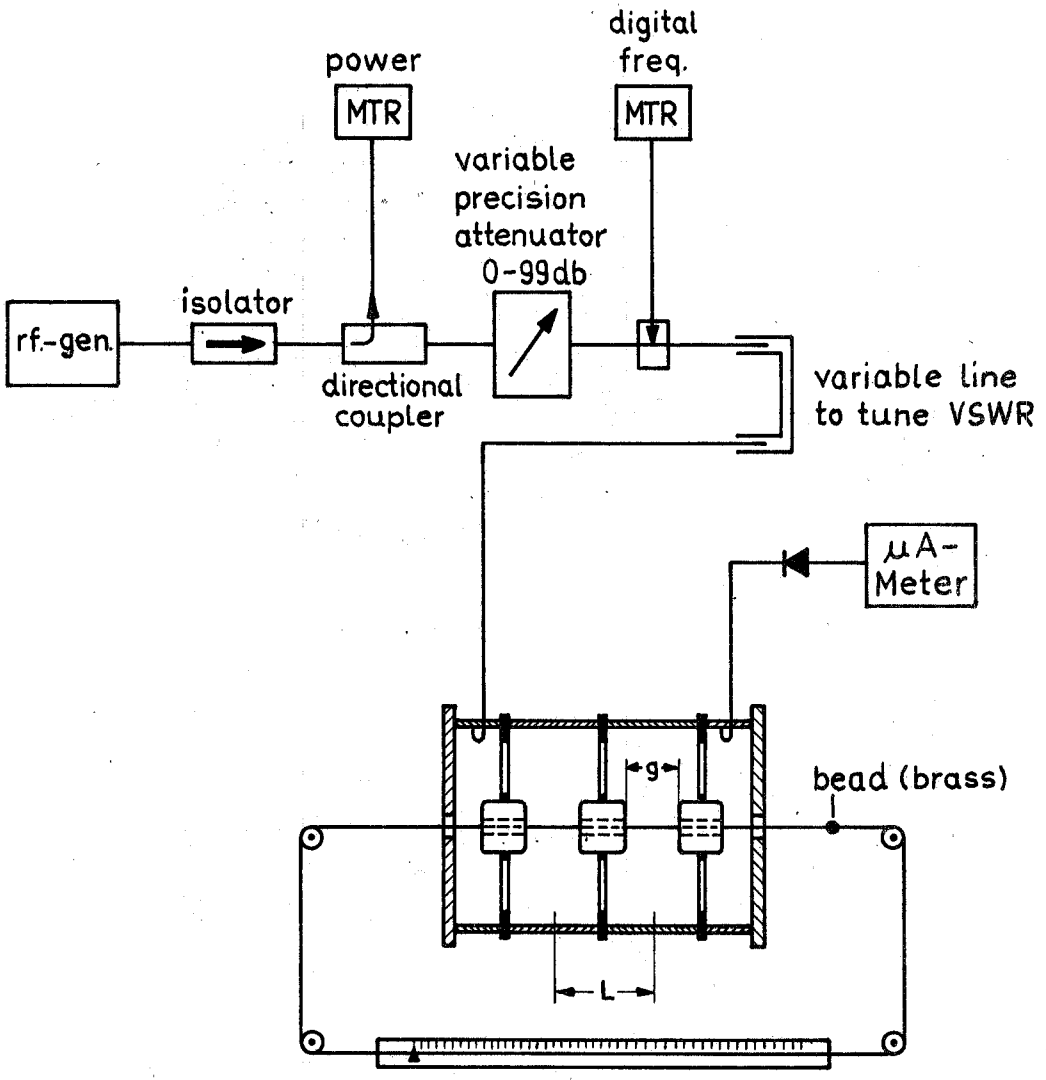
power
MTR
digital
freq.
MTR
variable
precision
attenuator
0-99db
isolator
rf.-gen.
directional
coupler
variable line
to tune VSWR
μA-
Meter
g
bead (brass)
L

Fig. 2

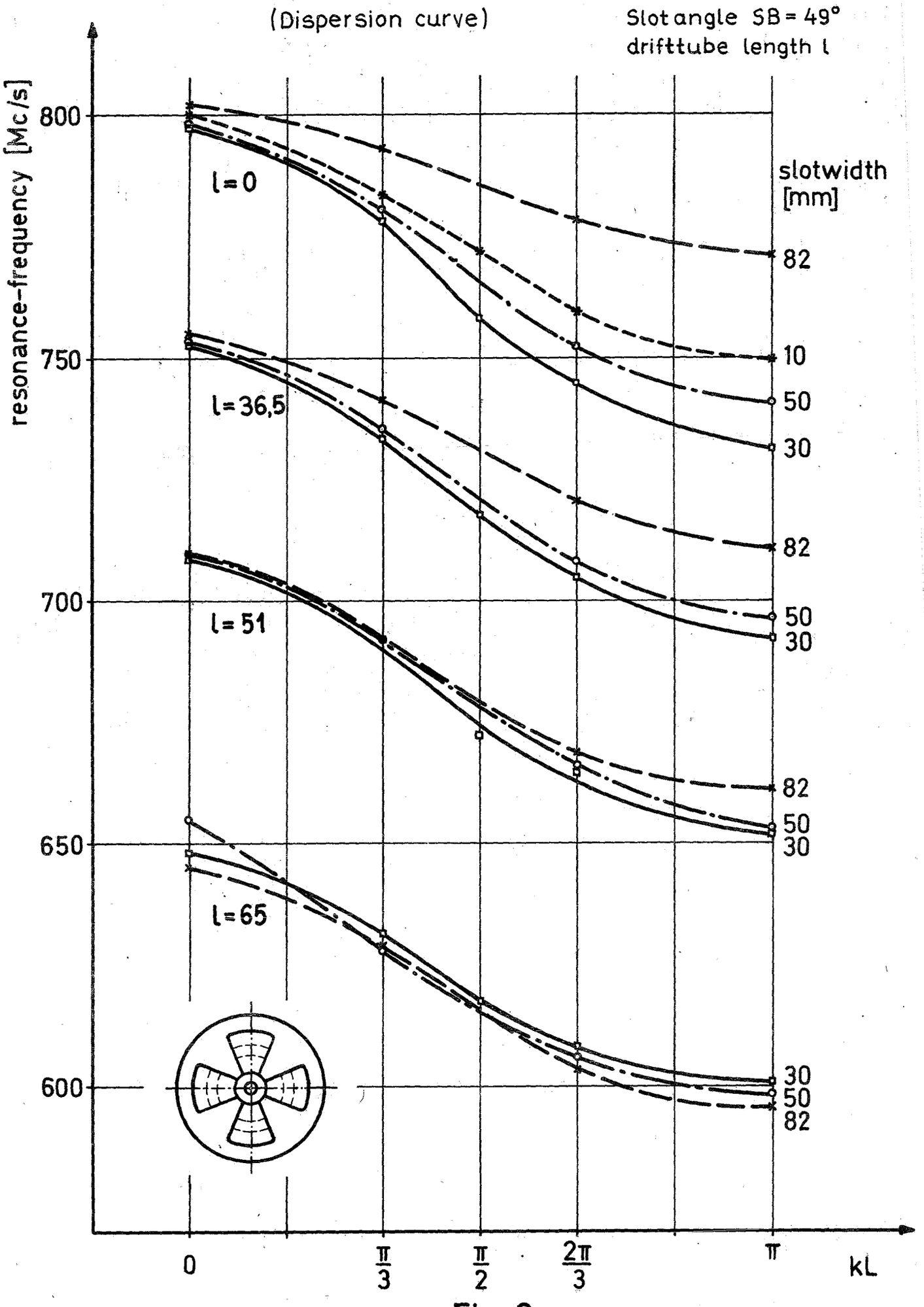
Slotted Iris (L= 98.8)
(Dispersion curve)
Slot angle SB = 49°
drifttube length l
resonance-frequency [Mc/s]
800
750
700
650
600
l=0
l=36,5
l=51
l=65
slotwidth [mm]
82
10
50
30
82
50
30
82
50
30
30
50
82
0
π/3
π/2
2π/3
π
kL

Fig. 3

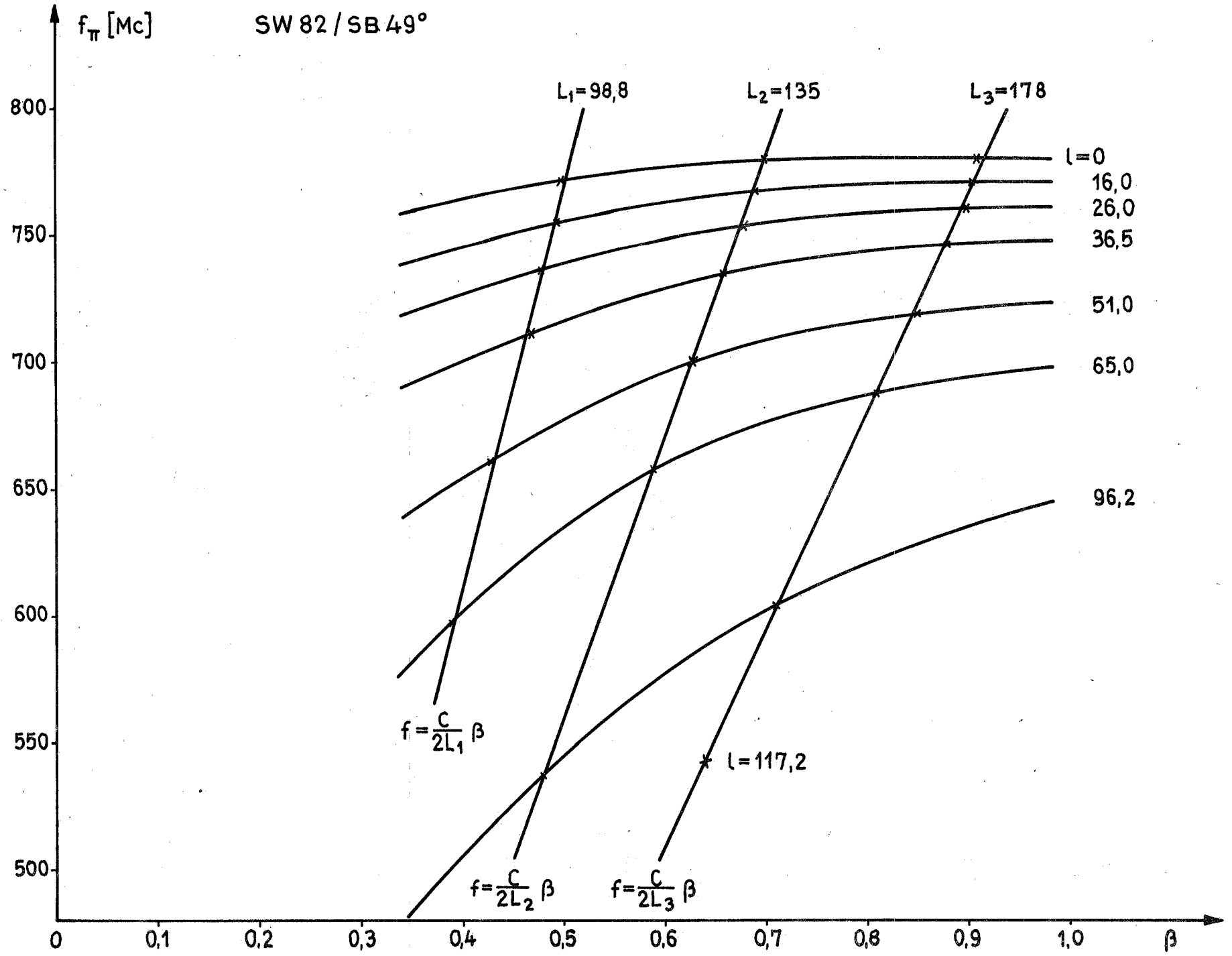
f_π [Mc]
SW 82 / SB 49°
800
750
700
650
600
550
500
0
0,1
0,2
0,3
0,4
0,5
0,6
0,7
0,8
0,9
1,0
β
L_1=98,8
L_2=135
L_3=178
l=0
16,0
26,0
36,5
51,0
65,0
96,2
l=117,2
$f=\frac{c}{2L_1}\beta$
$f=\frac{c}{2L_2}\beta$
$f=\frac{c}{2L_3}\beta$

Fig. 4

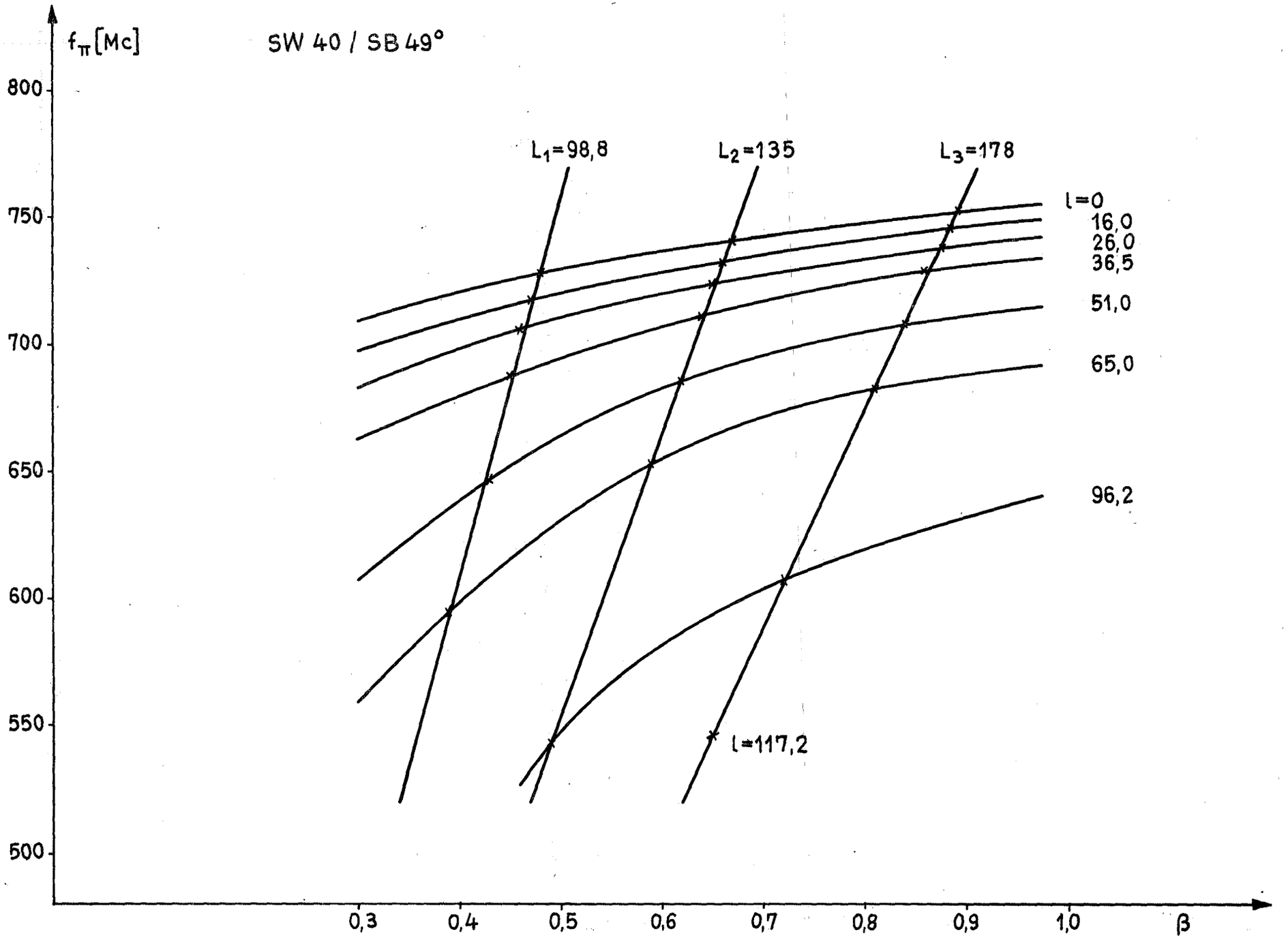
f_π[Mc]
SW 40 / SB 49°
800
750
700
650
600
550
500
L_1=98,8
L_2=135
L_3=178
l=0
16,0
26,0
36,5
51,0
65,0
96,2
l=117,2
0,3
0,4
0,5
0,6
0,7
0,8
0,9
1,0
β

Fig. 5

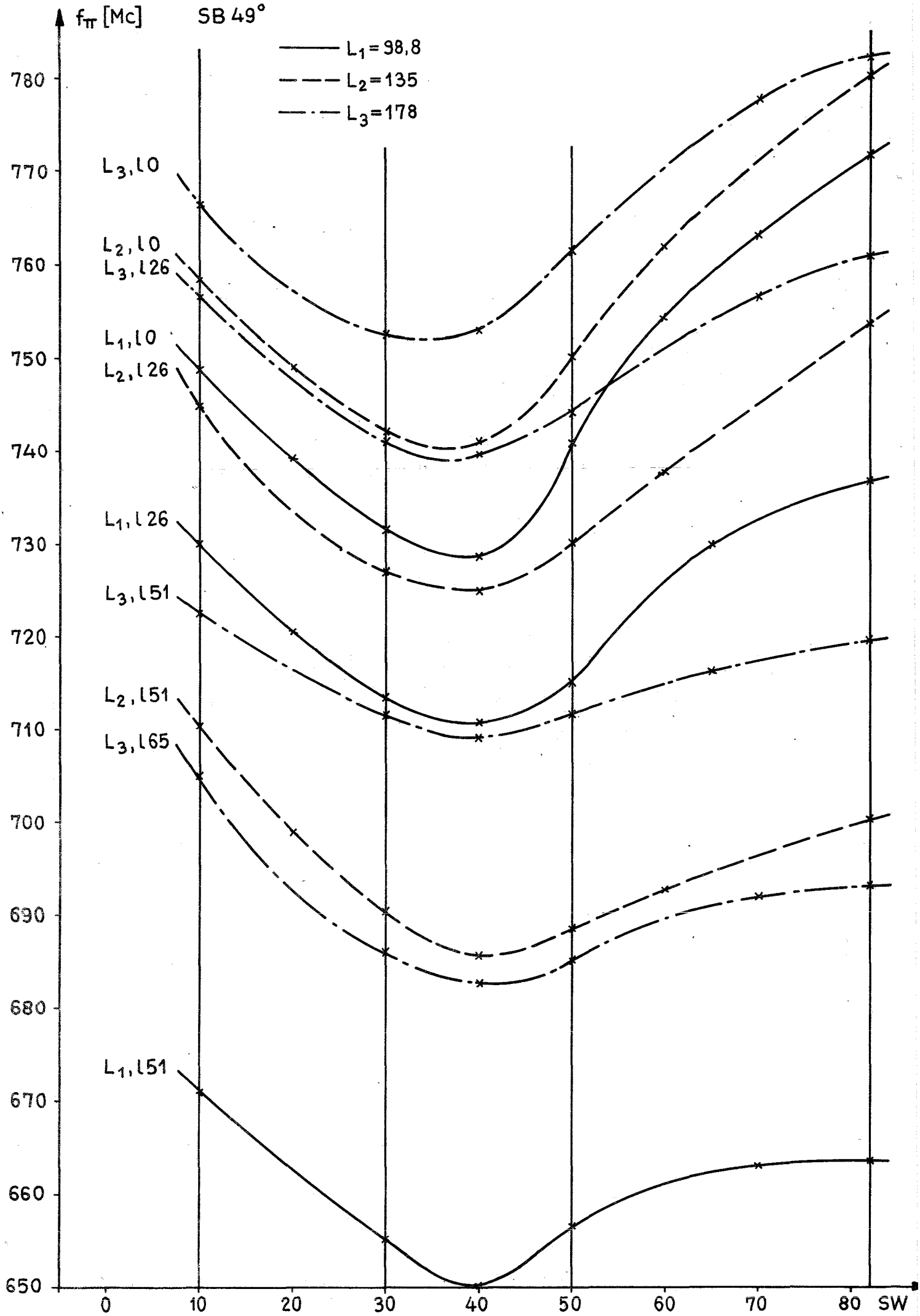
f_{π} [Mc]
SB 49°
L_1=98,8
L_2=135
L_3=178
780
770
760
750
740
730
720
710
700
690
680
670
660
650
L_3,l0
L_2,l0
L_3,l26
L_1,l0
L_2,l26
L_1,l26
L_3,l51
L_2,l51
L_3,l65
L_1,l51
0
10
20
30
40
50
60
70
80
SW

Fig. 8

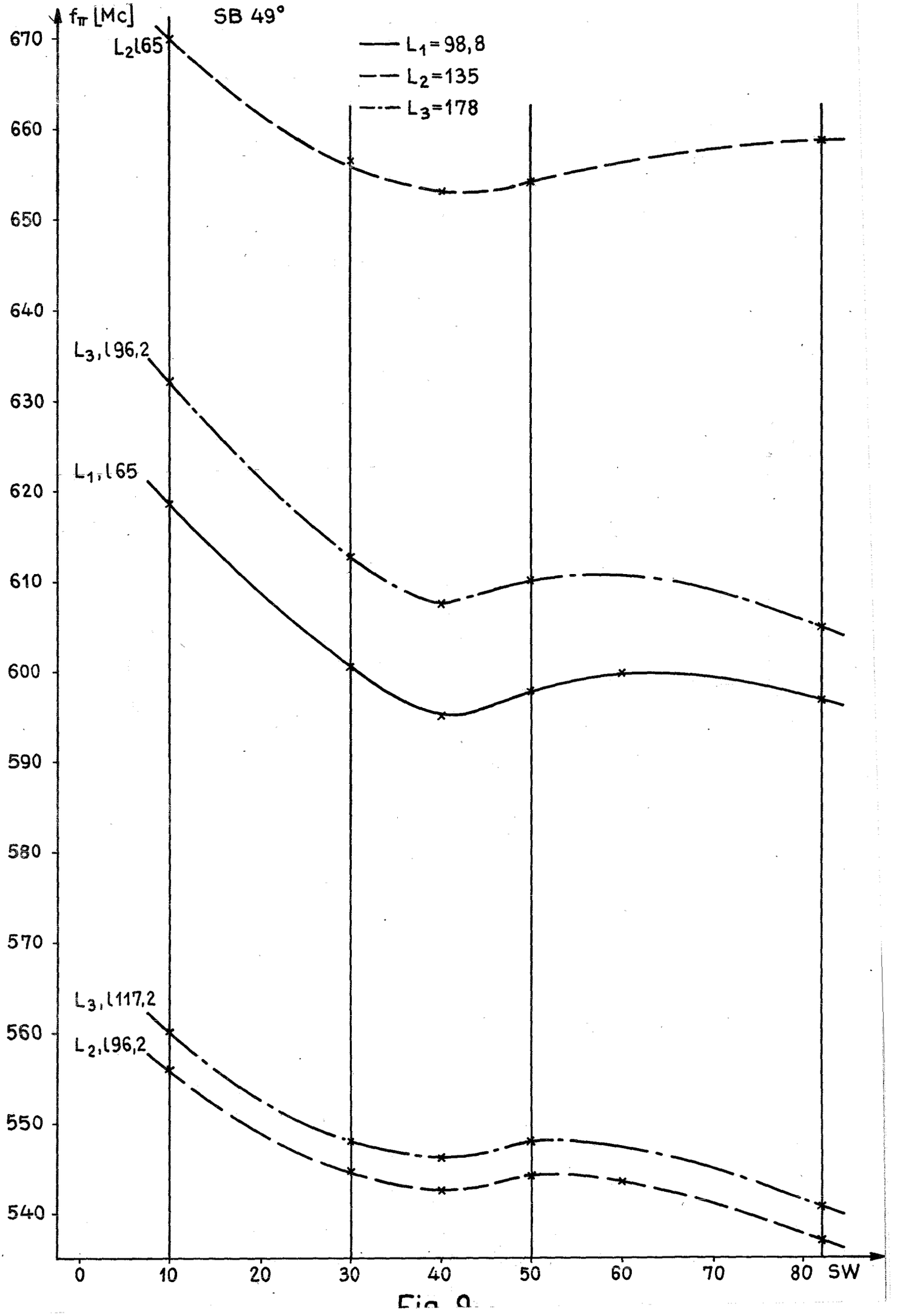
$f_{пр}$ [Mc]
SB 49°
L_1=98,8
L_2=135
L_3=178
L_2,l65
L_3,l96,2
L_1,l65
L_3,l117,2
L_2,l96,2
670
660
650
640
630
620
610
600
590
580
570
560
550
540
0
10
20
30
40
50
60
70
80
SW

Fig. 9

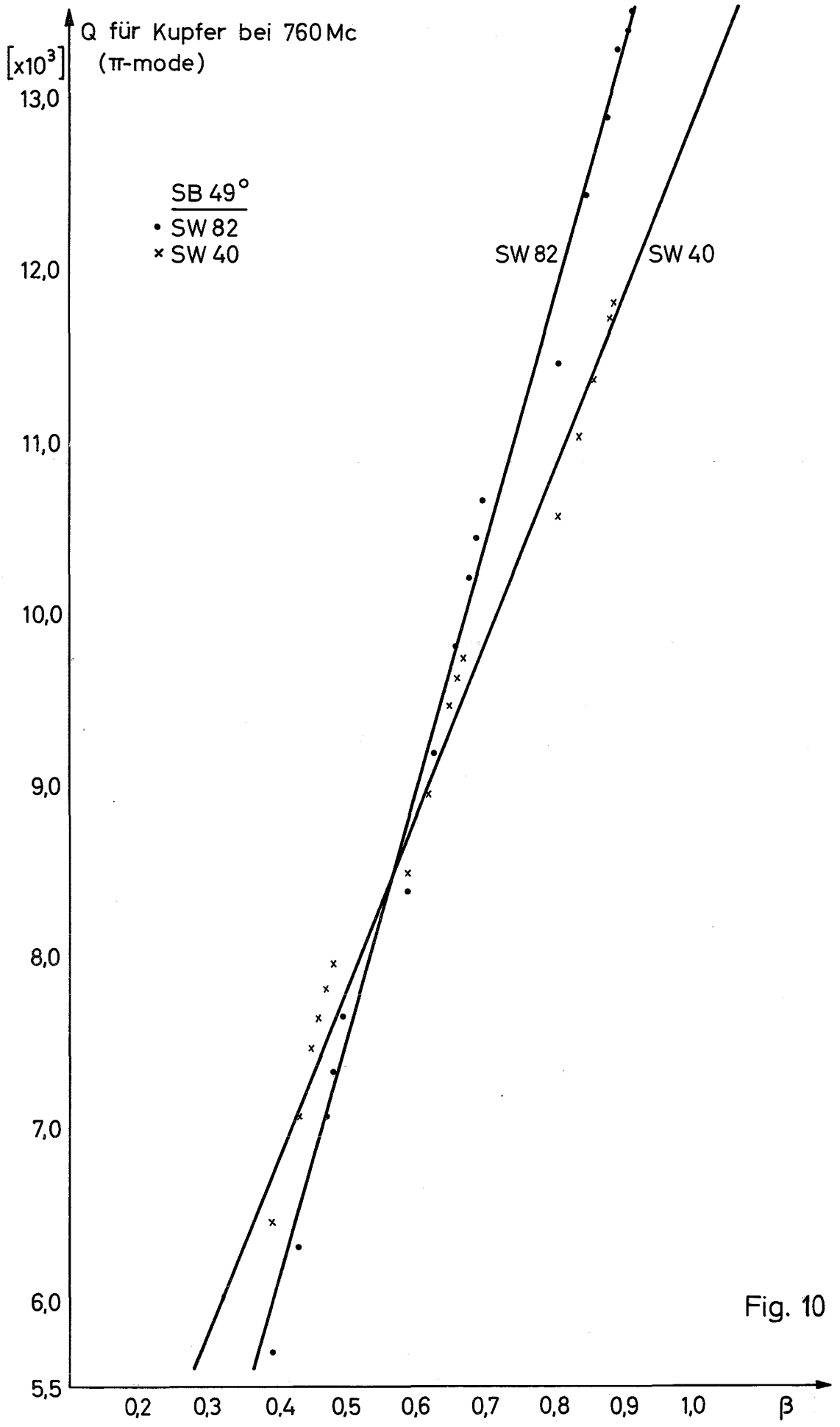
Q für Kupfer bei 760 Mc
(π-mode)
[x10³]
13,0
12,0
11,0
10,0
9,0
8,0
7,0
6,0
5,5
SB 49°
• SW 82
× SW 40
SW 82
SW 40
0,2
0,3
0,4
0,5
0,6
0,7
0,8
0,9
1,0
β

Fig. 10

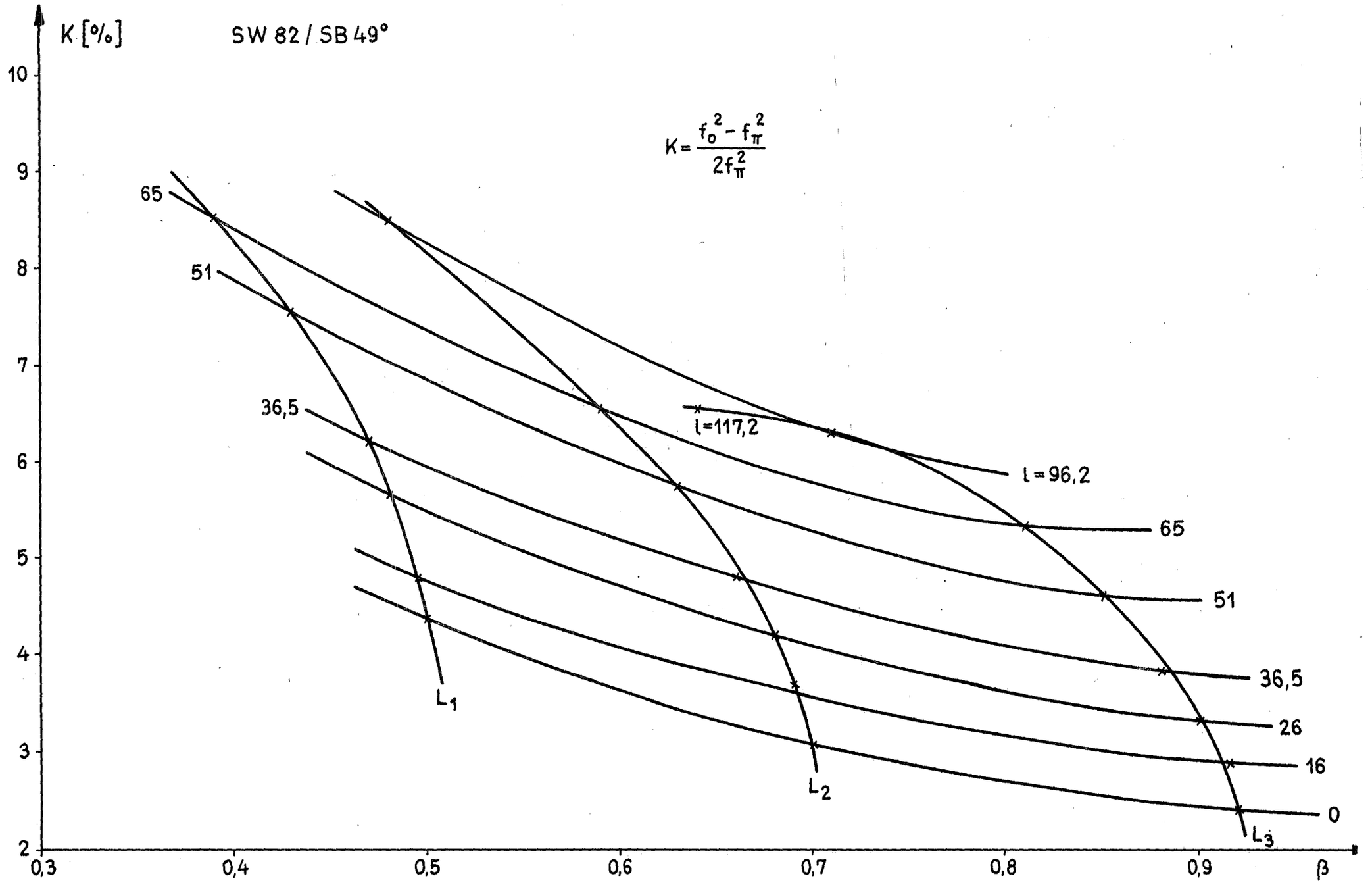
K [%]
SW 82 / SB 49°
$K = \frac{f_o^2 - f_\pi^2}{2f_\pi^2}$
10
9
8
7
6
5
4
3
2
0,3
0,4
0,5
0,6
0,7
0,8
0,9
β
65
51
36,5
l=117,2
l=96,2
65
51
36,5
26
16
0
L_1
L_2
L_3

Fig. 11

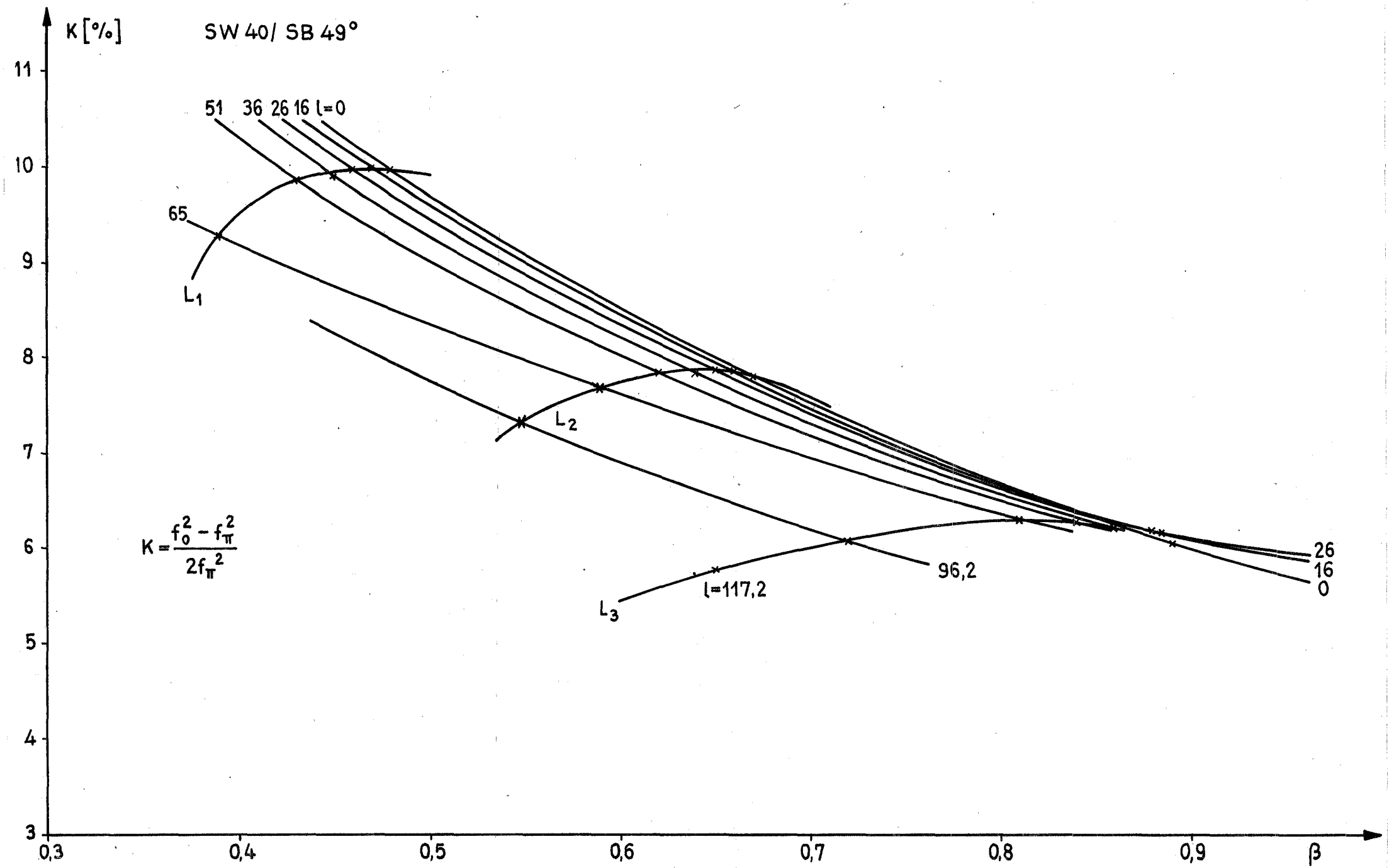
K [%]
SW 40/ SB 49°
11
10
9
8
7
6
5
4
3
0,3
0,4
0,5
0,6
0,7
0,8
0,9
β
51
36
26
16
l=0
65
L1
L2
L3
96,2
l=117,2
26
16
0
$K = \frac{f_o^2 - f_\pi^2}{2 f_\pi^2}$

Fig. 12

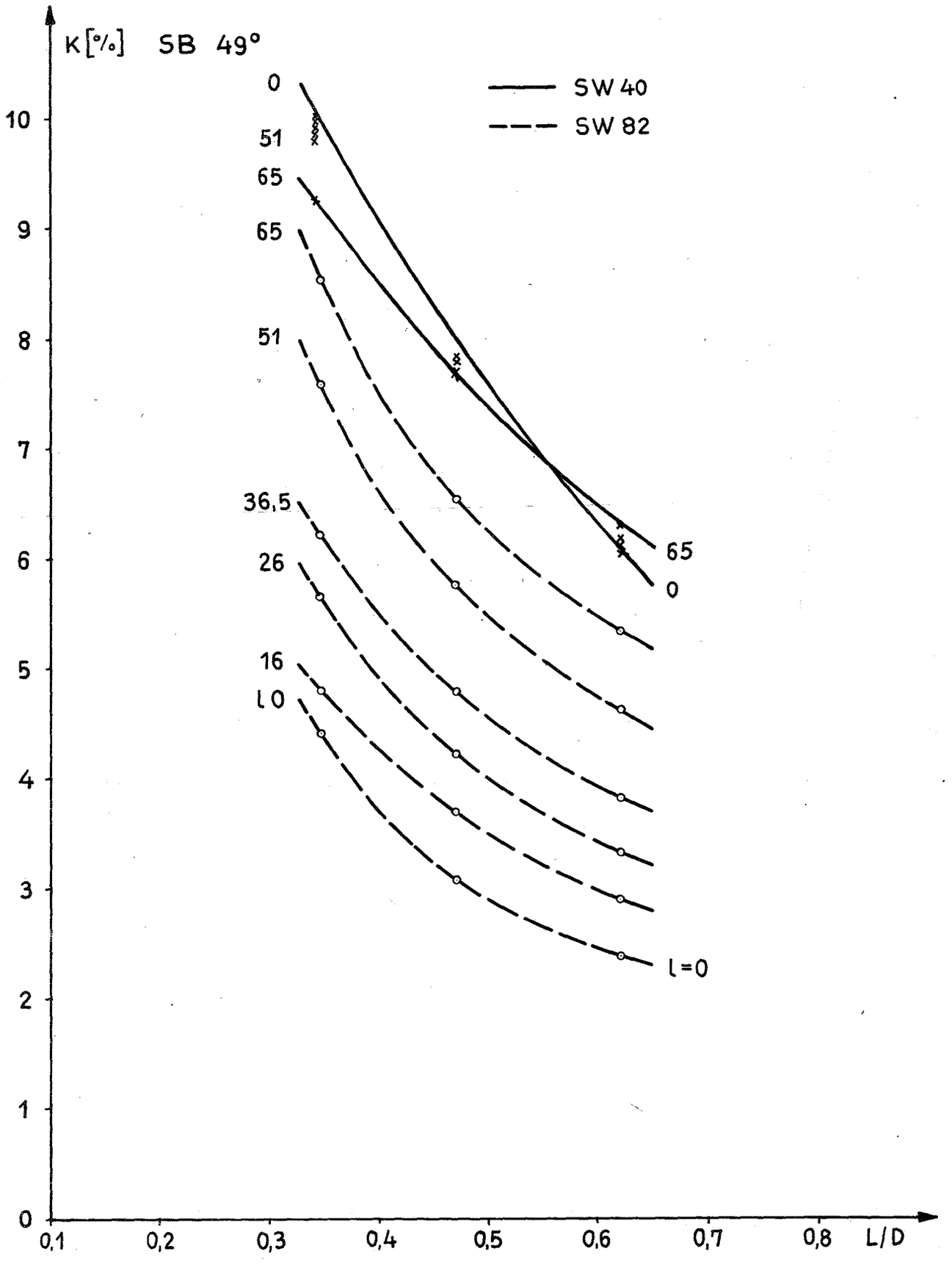
K[%] SB 49°
SW 40
SW 82
0
51
65
65
51
36,5
26
16
10
0
65
0
l=0
10
9
8
7
6
5
4
3
2
1
0
0,1
0,2
0,3
0,4
0,5
0,6
0,7
0,8
L/D

Fig. 13

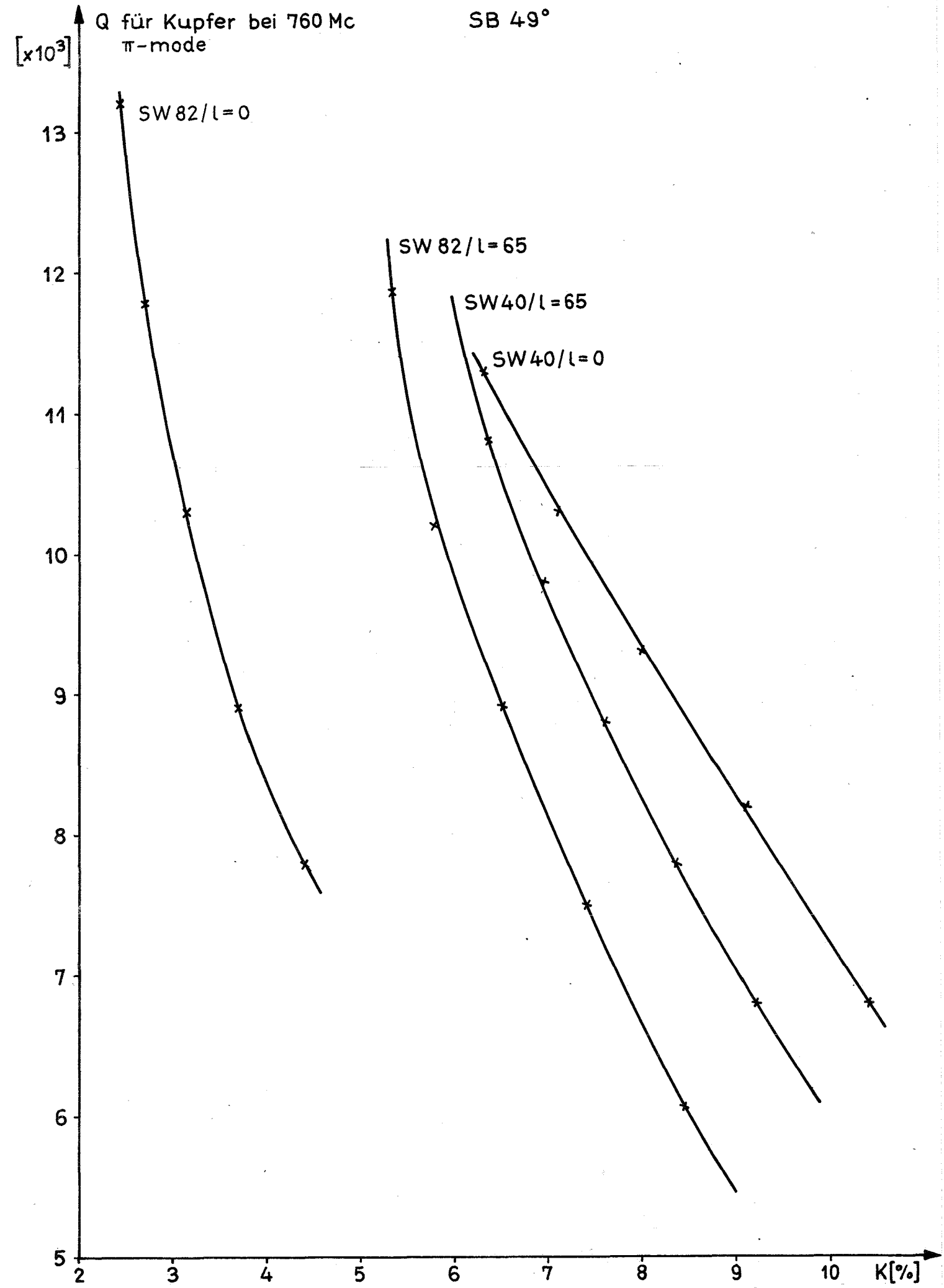
Q für Kupfer bei 760 Mc
π-mode
SB 49°
[x10³]
SW 82/l=0
SW 82/l=65
SW40/l=65
SW40/l=0
13
12
11
10
9
8
7
6
5
2
3
4
5
6
7
8
9
10
K[%]

Fig. 14

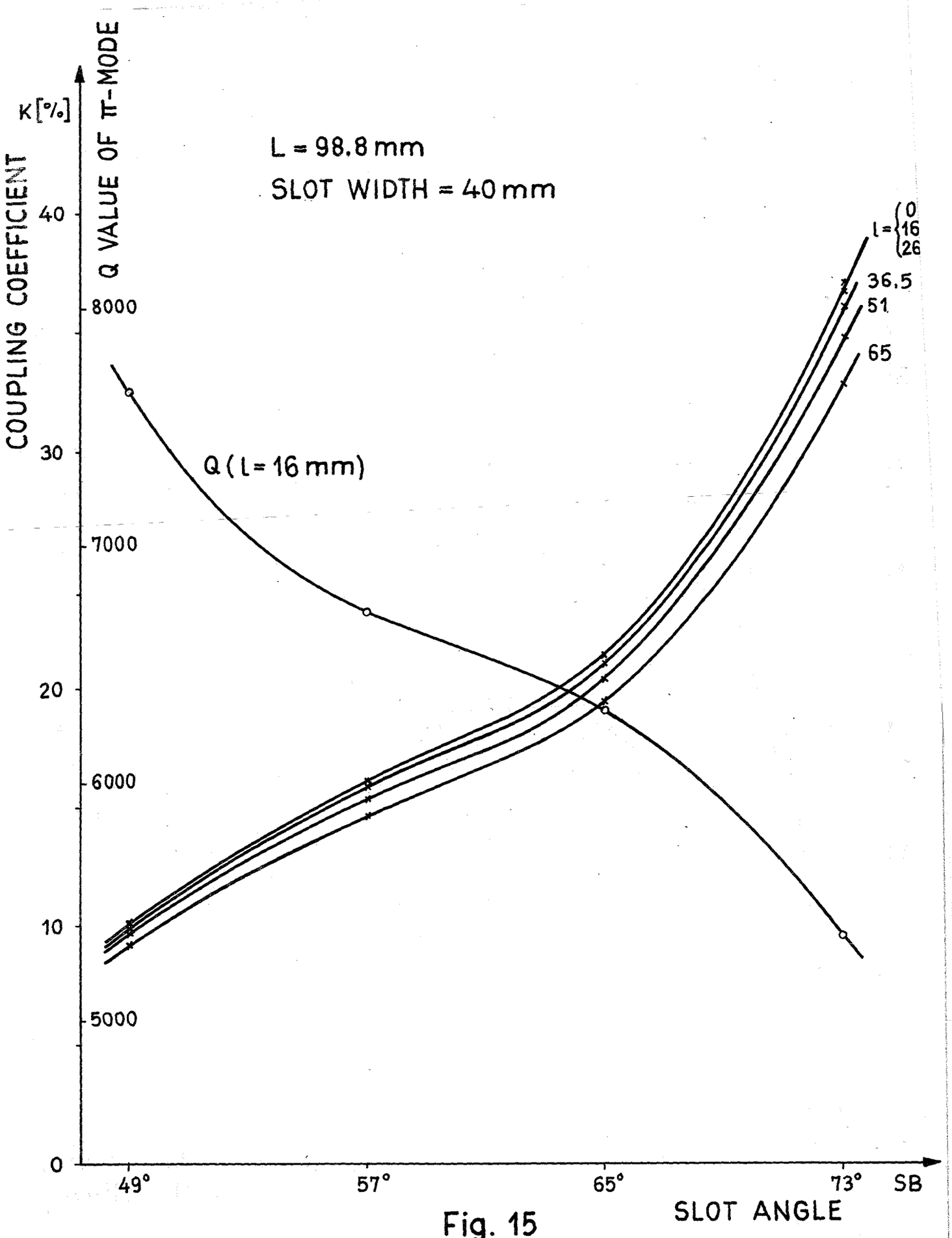
COUPLING COEFFICIENT
K[%]
Q VALUE OF π-MODE
L = 98.8 mm
SLOT WIDTH = 40 mm
l = 0
16
26
36.5
51
65
Q (l = 16 mm)
40
30
20
10
0
8000
7000
6000
5000
49°
57°
65°
73°
SB
SLOT ANGLE

Fig. 15

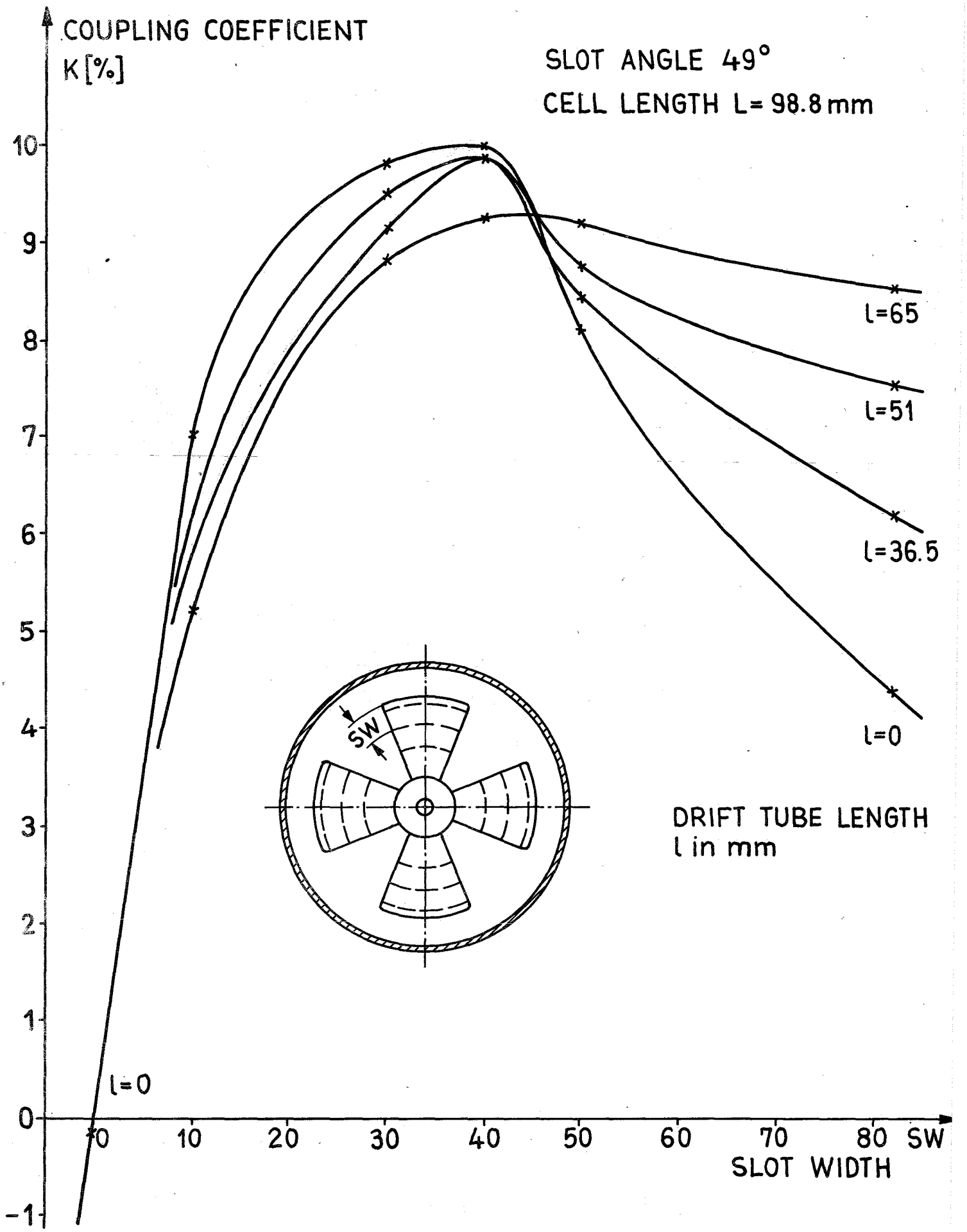
COUPLING COEFFICIENT
K[%]
SLOT ANGLE 49°
CELL LENGTH L= 98.8 mm
10
9
8
7
6
5
4
3
2
1
0
-1
l=65
l=51
l=36.5
l=0
l=0
SW
DRIFT TUBE LENGTH
l in mm
0
10
20
30
40
50
60
70
80
SW
SLOT WIDTH

Fig. 16

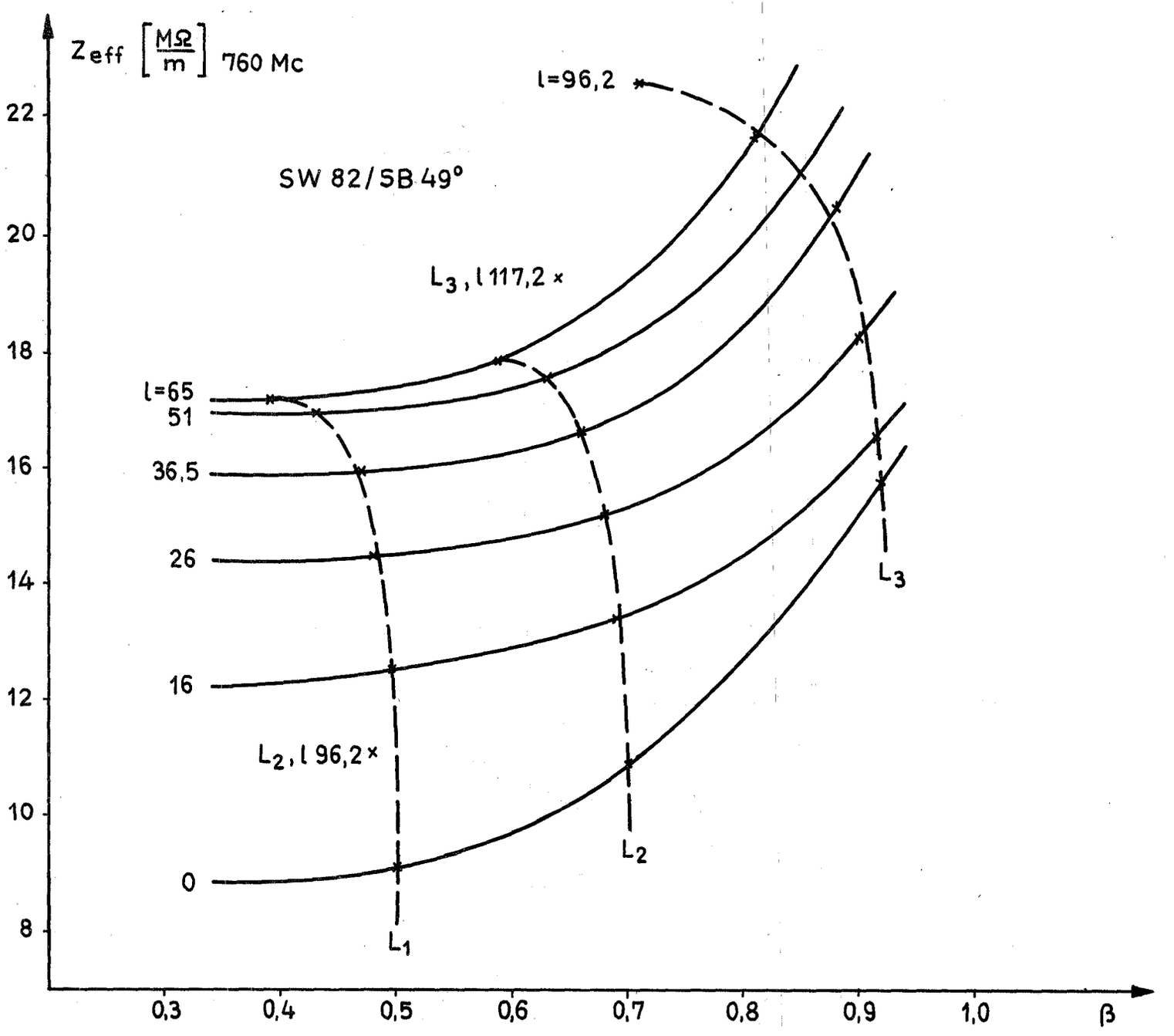
Zeff [MΩ/m] 760 Mc
l=96,2
SW 82/SB 49°
L3, l 117,2 x
l=65
51
36,5
26
16
0
L2, l 96,2 x
L1
L2
L3
22
20
18
16
14
12
10
8
0,3
0,4
0,5
0,6
0,7
0,8
0,9
1,0
β

Fig. 17

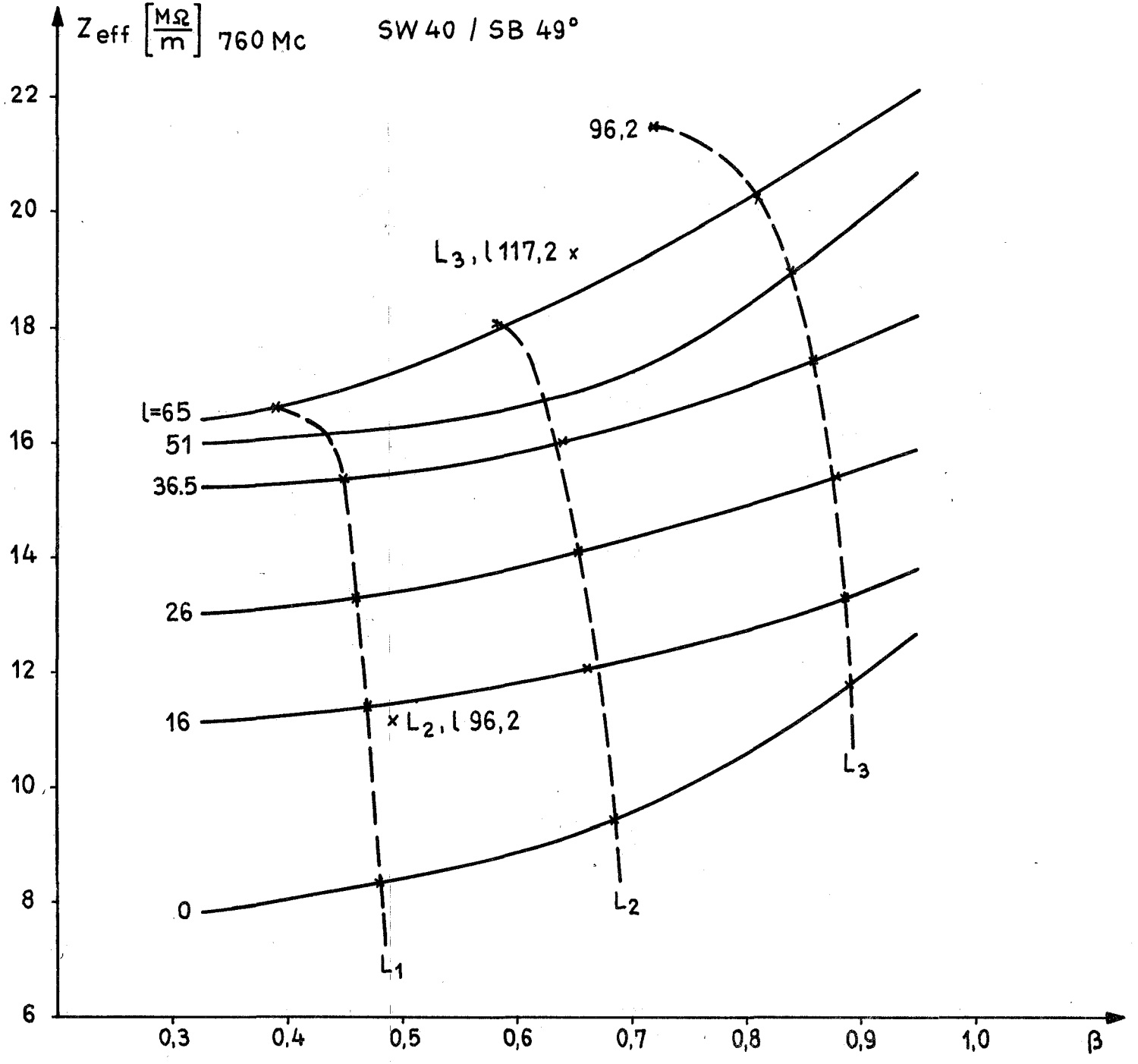
Z eff [MΩ/m] 760 Mc
SW 40 / SB 49°
22
20
18
16
14
12
10
8
6
96,2
L3, l 117,2 x
l=65
51
36.5
26
16
0
x L2, l 96,2
L1
L2
L3
0,3
0,4
0,5
0,6
0,7
0,8
0,9
1,0
β

Fig. 18

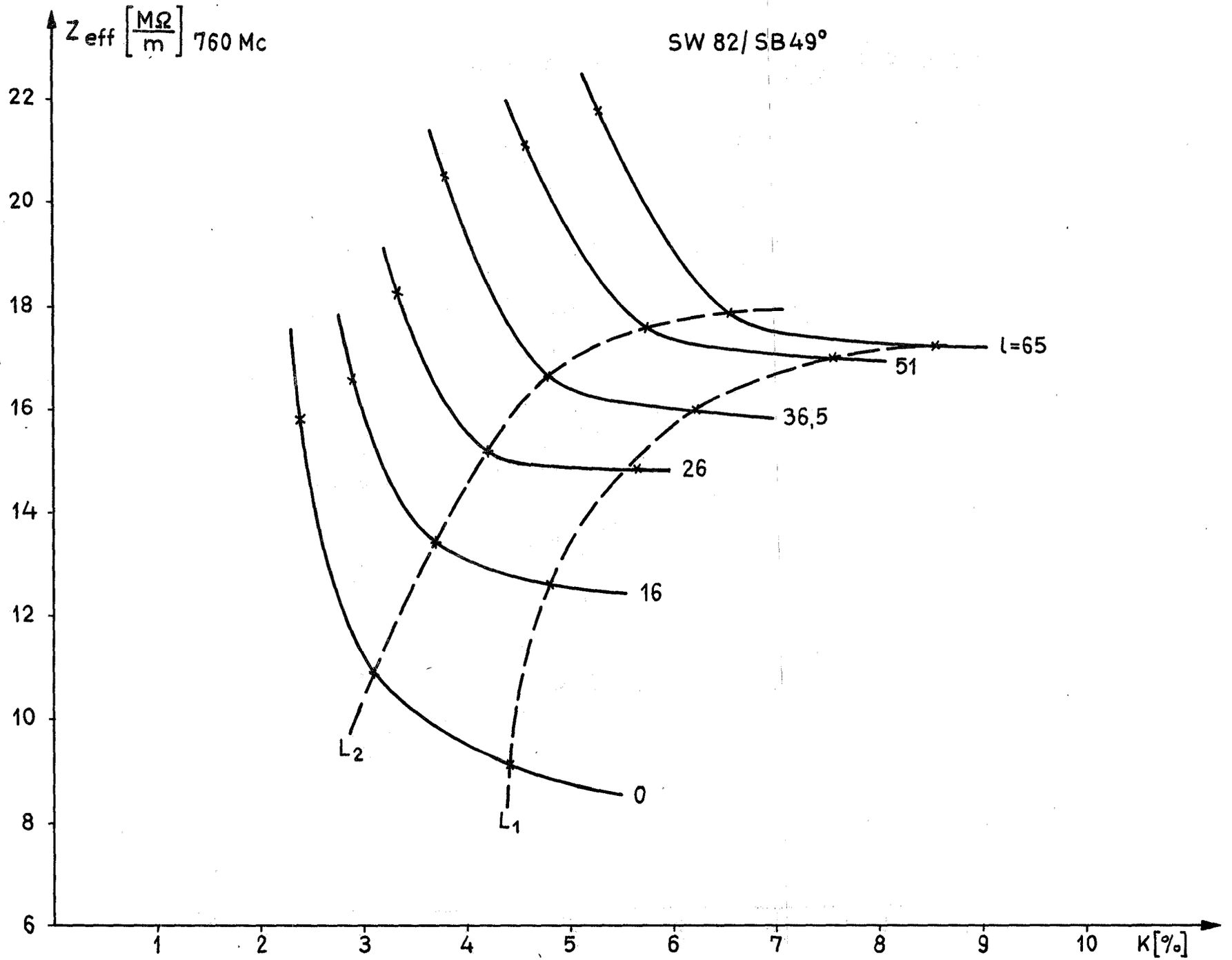
Z eff [MΩ/m] 760 Mc
SW 82/ SB 49°
22
20
18
16
14
12
10
8
6
1
2
3
4
5
6
7
8
9
10
K[%]
l=65
51
36,5
26
16
0
L2
L1

Fig. 19

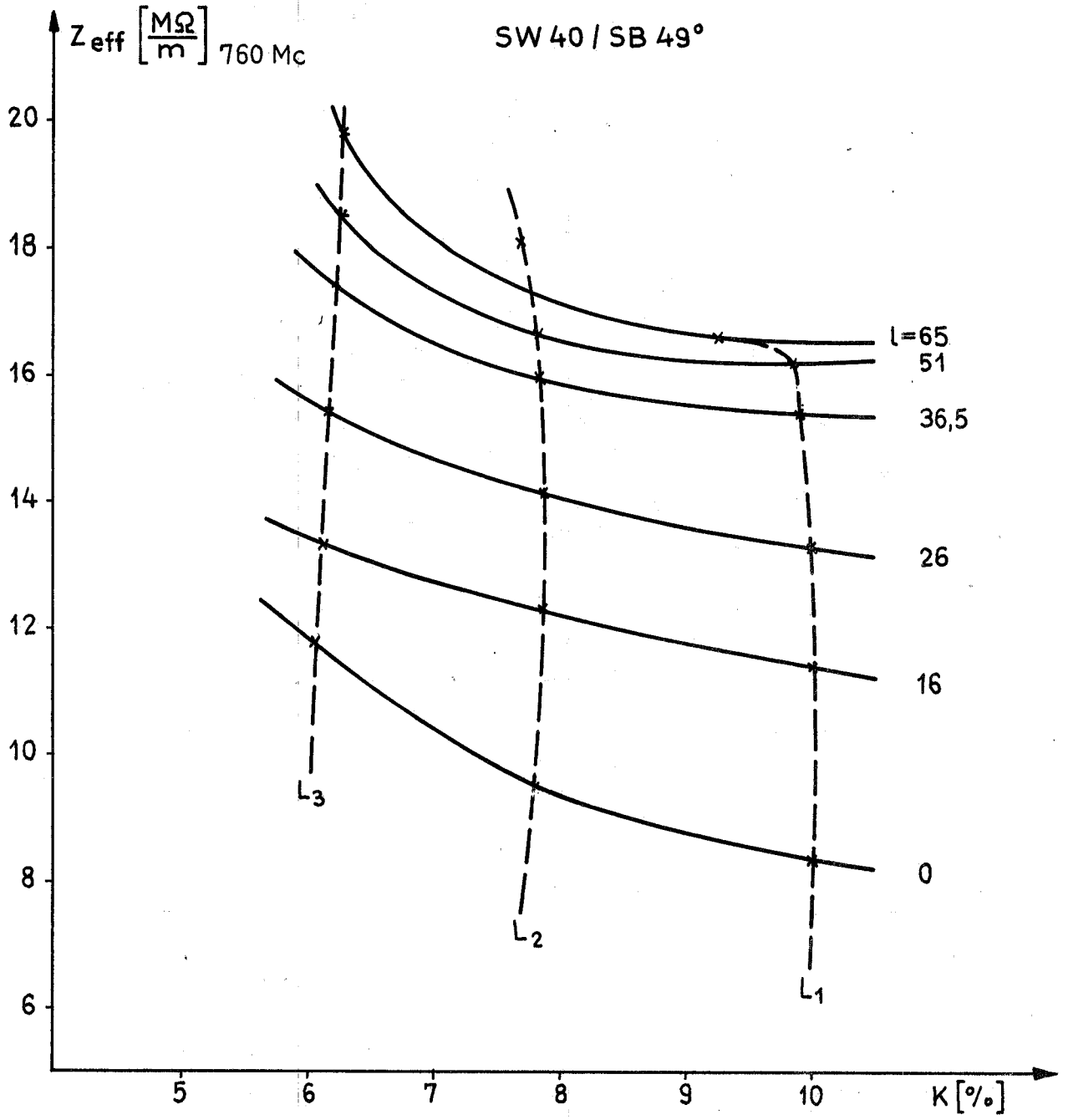
$Z_{eff}\left[\frac{M\Omega}{m}\right]$ 760 Mc
SW 40 / SB 49°
20
18
16
14
12
10
8
6
5
6
7
8
9
10
K [%]
l=65
51
36,5
26
16
0
L_1
L_2
L_3

Fig. 20

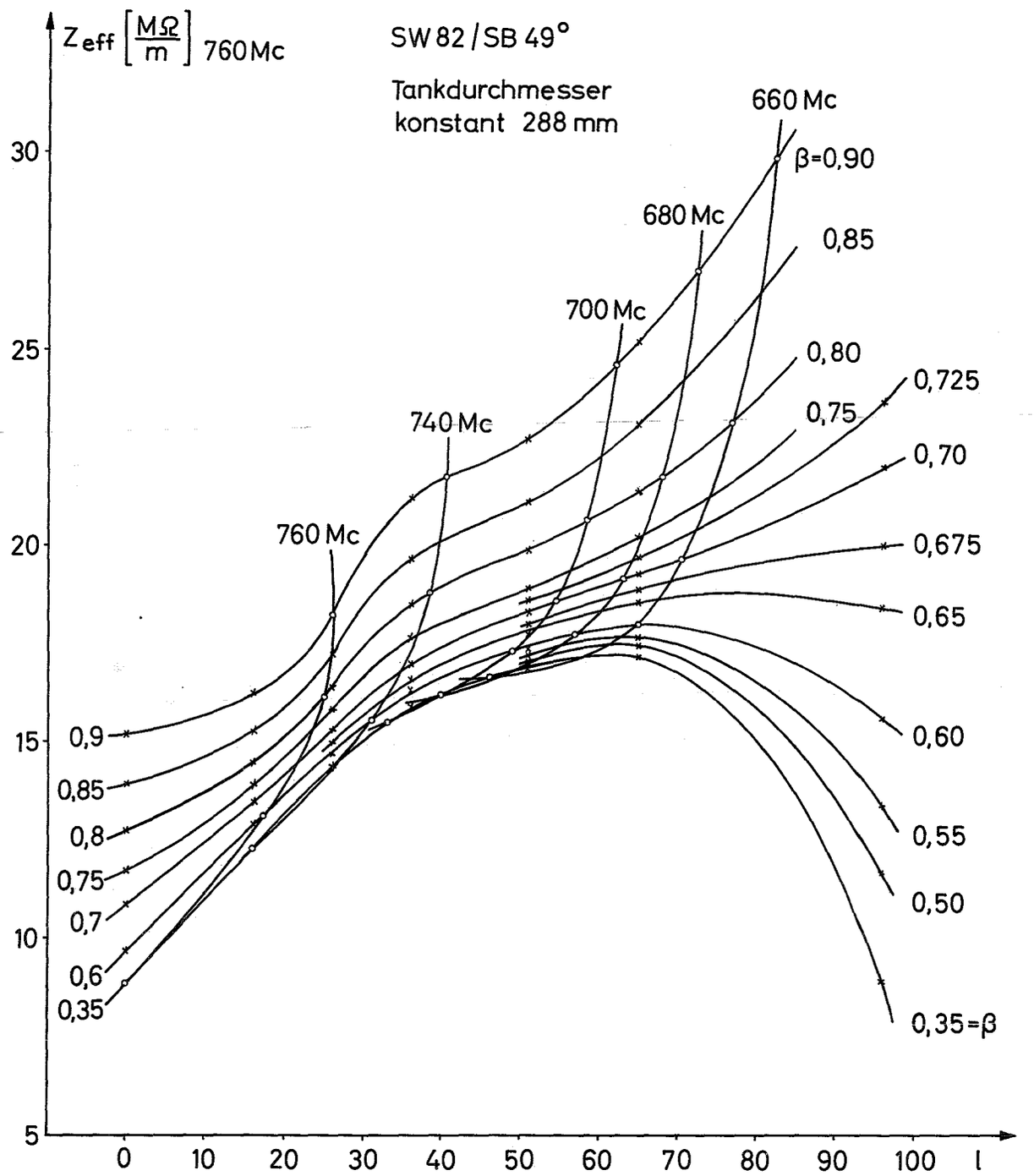
$Z_{eff}\left[\frac{M\Omega}{m}\right]$ 760 Mc
SW 82 / SB 49°
Tankdurchmesser
konstant 288 mm
660 Mc
β=0,90
680 Mc
0,85
700 Mc
0,80
0,725
740 Mc
0,75
0,70
760 Mc
0,675
0,65
0,60
0,55
0,50
0,35=β
0,9
0,85
0,8
0,75
0,7
0,6
0,35
30
25
20
15
10
5
0
10
20
30
40
50
60
70
80
90
100
l

Fig. 21

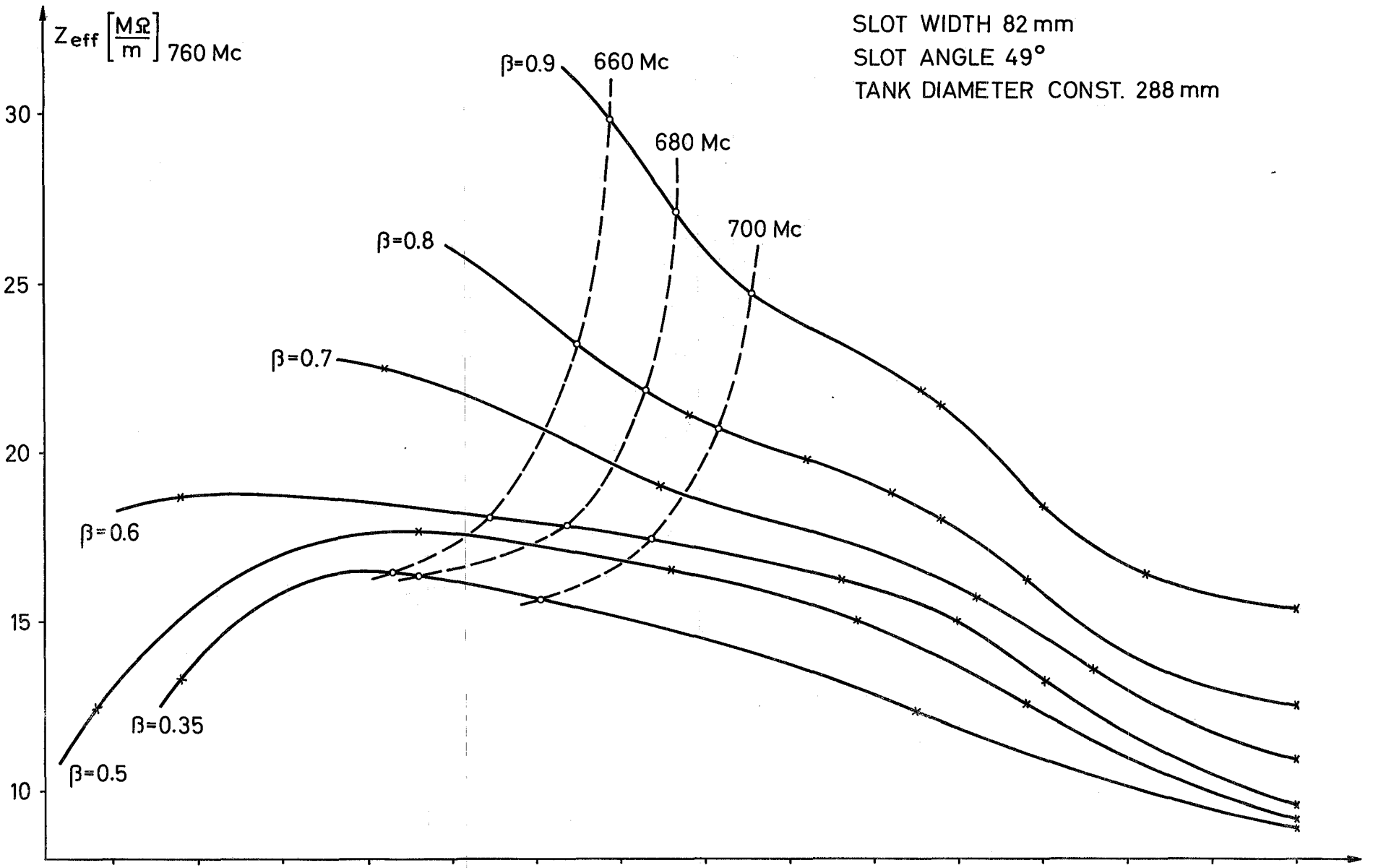
$Z_{eff}\left[\frac{M\Omega}{m}\right]$ 760 Mc
SLOT WIDTH 82 mm
SLOT ANGLE 49°
TANK DIAMETER CONST. 288 mm
β=0.9
660 Mc
680 Mc
700 Mc
β=0.8
β=0.7
β=0.6
β=0.35
β=0.5
30
25
20
15
10
0.3
0.4
0.5
0.6
0.7
0.8
0.9
1.0 g/L
GAP LENGTH/CELL LENGTH

Fig. 21a

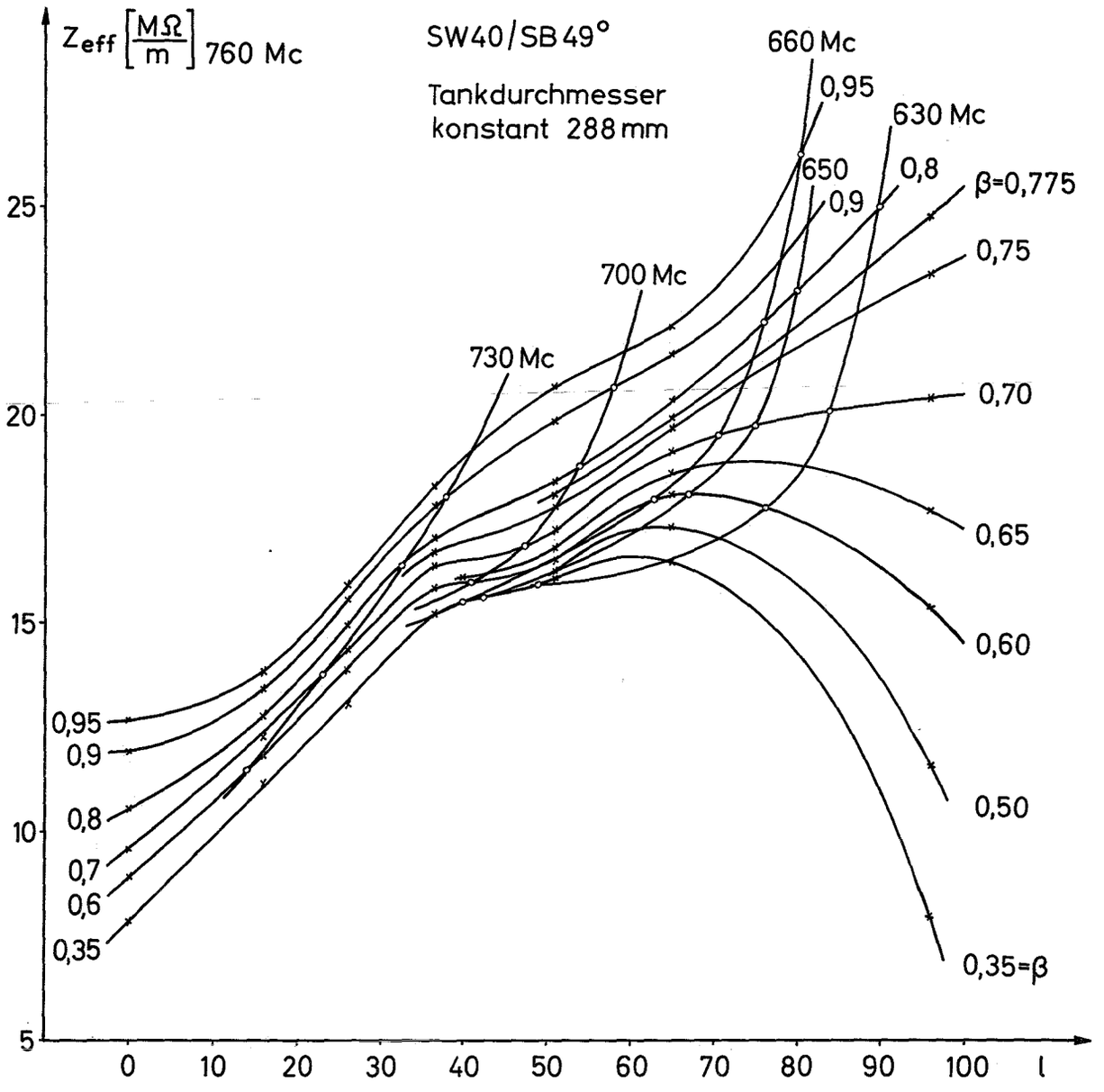
$Z_{eff}\left[\frac{M\Omega}{m}\right]$ 760 Mc
SW40/SB 49°
Tankdurchmesser
konstant 288 mm
660 Mc
0,95
630 Mc
650
0,8
β=0,775
0,9
0,75
700 Mc
730 Mc
0,70
0,65
0,60
0,50
0,35=β
0,95
0,9
0,8
0,7
0,6
0,35
25
20
15
10
5
0
10
20
30
40
50
60
70
80
90
100
l

Fig. 22

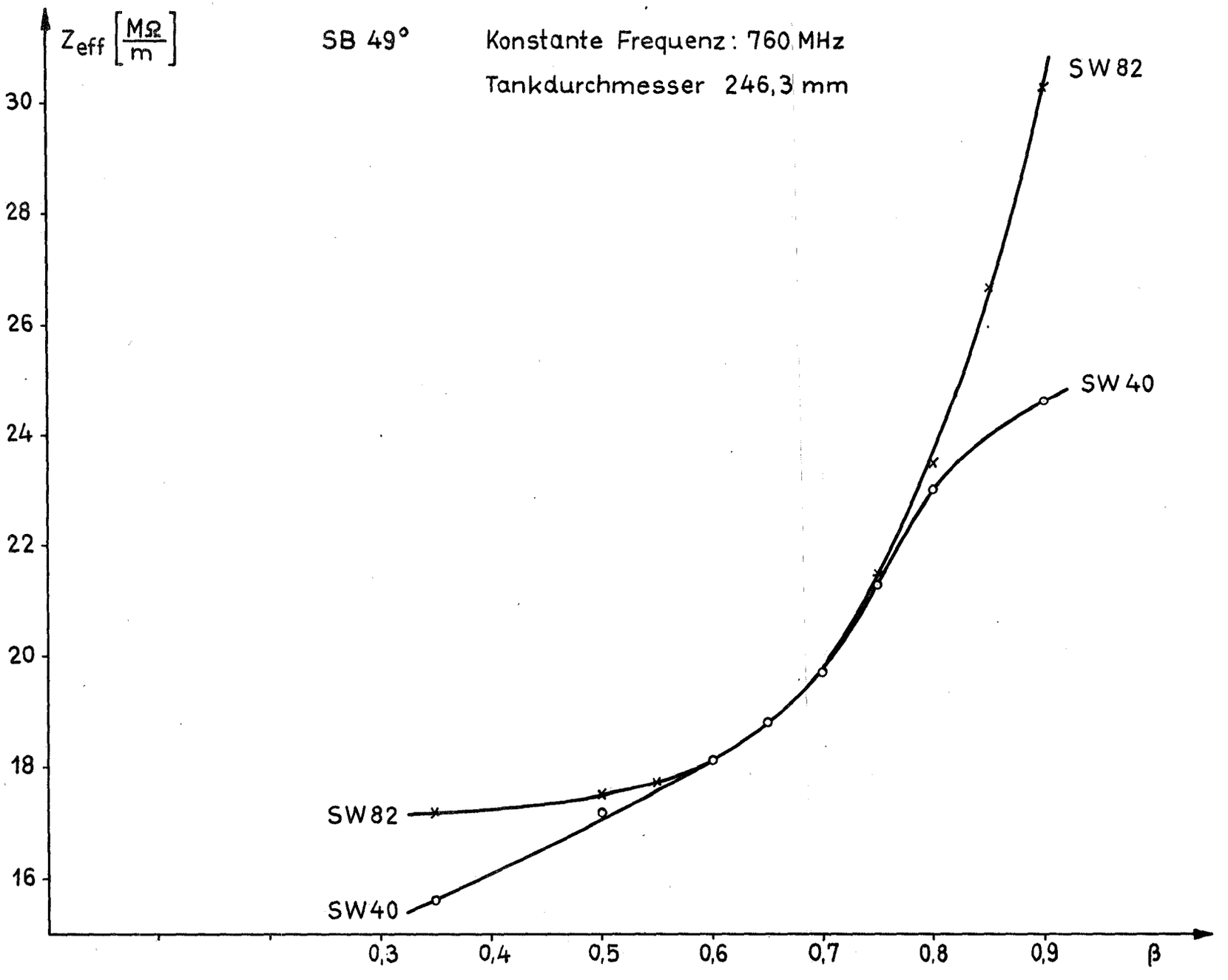
$Z_{eff}\left[\frac{M\Omega}{m}\right]$
SB 49°
Konstante Frequenz: 760 MHz
Tankdurchmesser 246,3 mm
SW 82
SW 40
SW82
SW40
30
28
26
24
22
20
18
16
0,3
0,4
0,5
0,6
0,7
0,8
0,9
β

Fig. 23

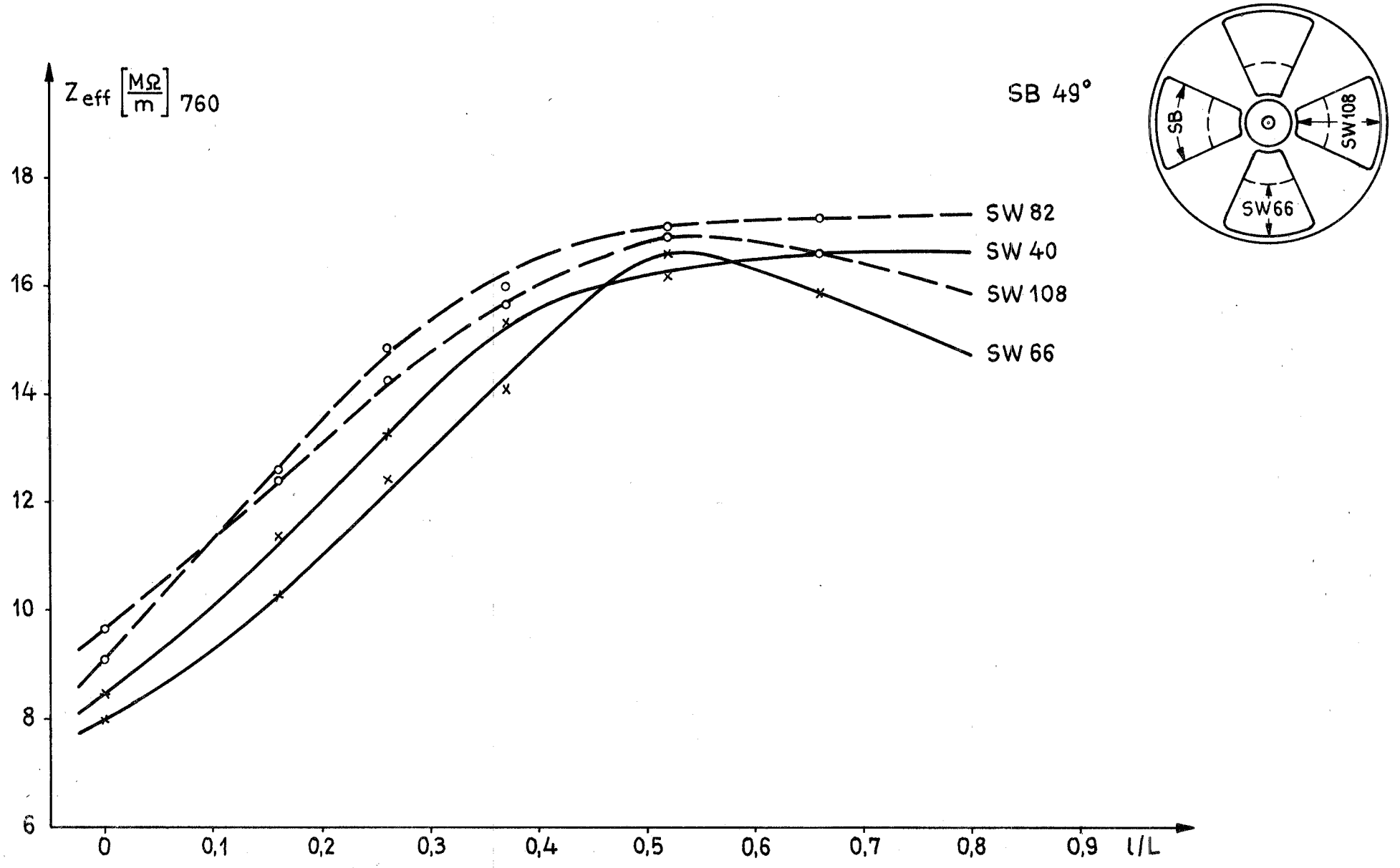
Z_{eff} $\left[\frac{M\Omega}{m}\right]$ 760
SB 49°
SW 82
SW 40
SW 108
SW 66
SB
SW108
SW66
18
16
14
12
10
8
6
0
0,1
0,2
0,3
0,4
0,5
0,6
0,7
0,8
0,9
l/L

Fig. 24

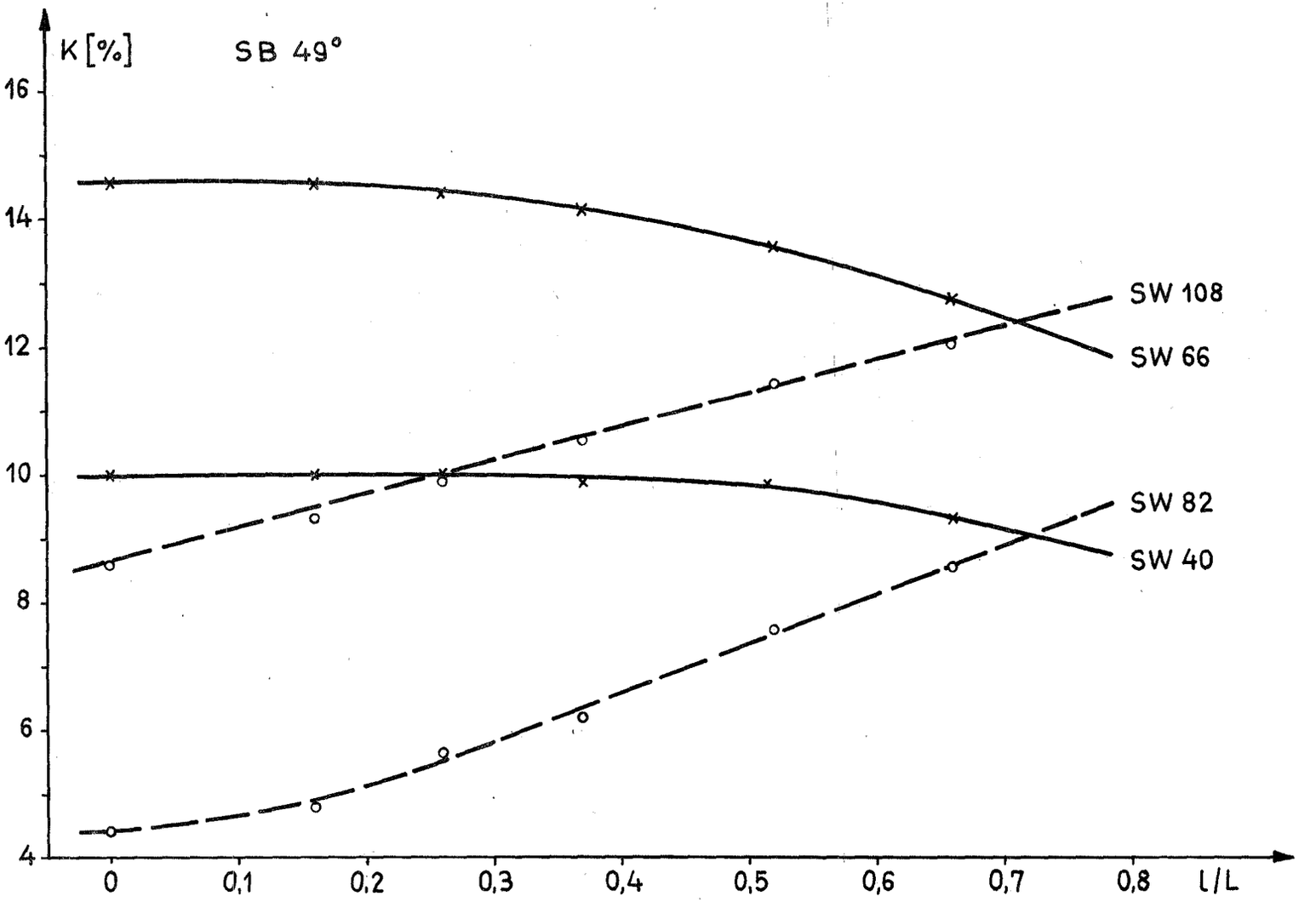
K [%]
SB 49°
16
14
12
10
8
6
4
0
0,1
0,2
0,3
0,4
0,5
0,6
0,7
0,8
L/L
SW 108
SW 66
SW 82
SW 40

Fig. 25

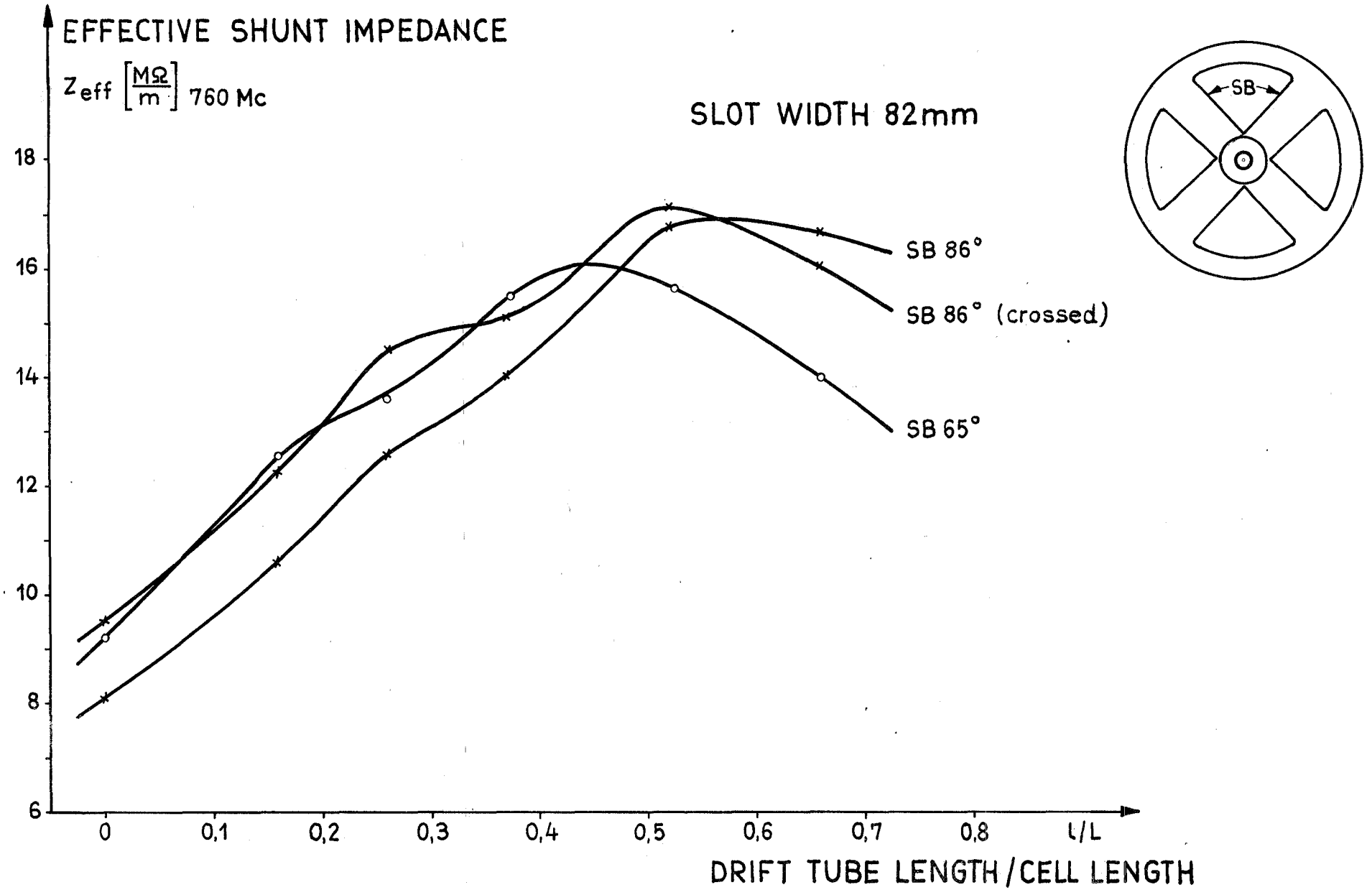
EFFECTIVE SHUNT IMPEDANCE
Z_{eff} $\left[\frac{M\Omega}{m}\right]$ 760 Mc
SLOT WIDTH 82mm
SB
SB 86°
SB 86° (crossed)
SB 65°
18
16
14
12
10
8
6
0
0,1
0,2
0,3
0,4
0,5
0,6
0,7
0,8
l/L
DRIFT TUBE LENGTH / CELL LENGTH

Fig. 26

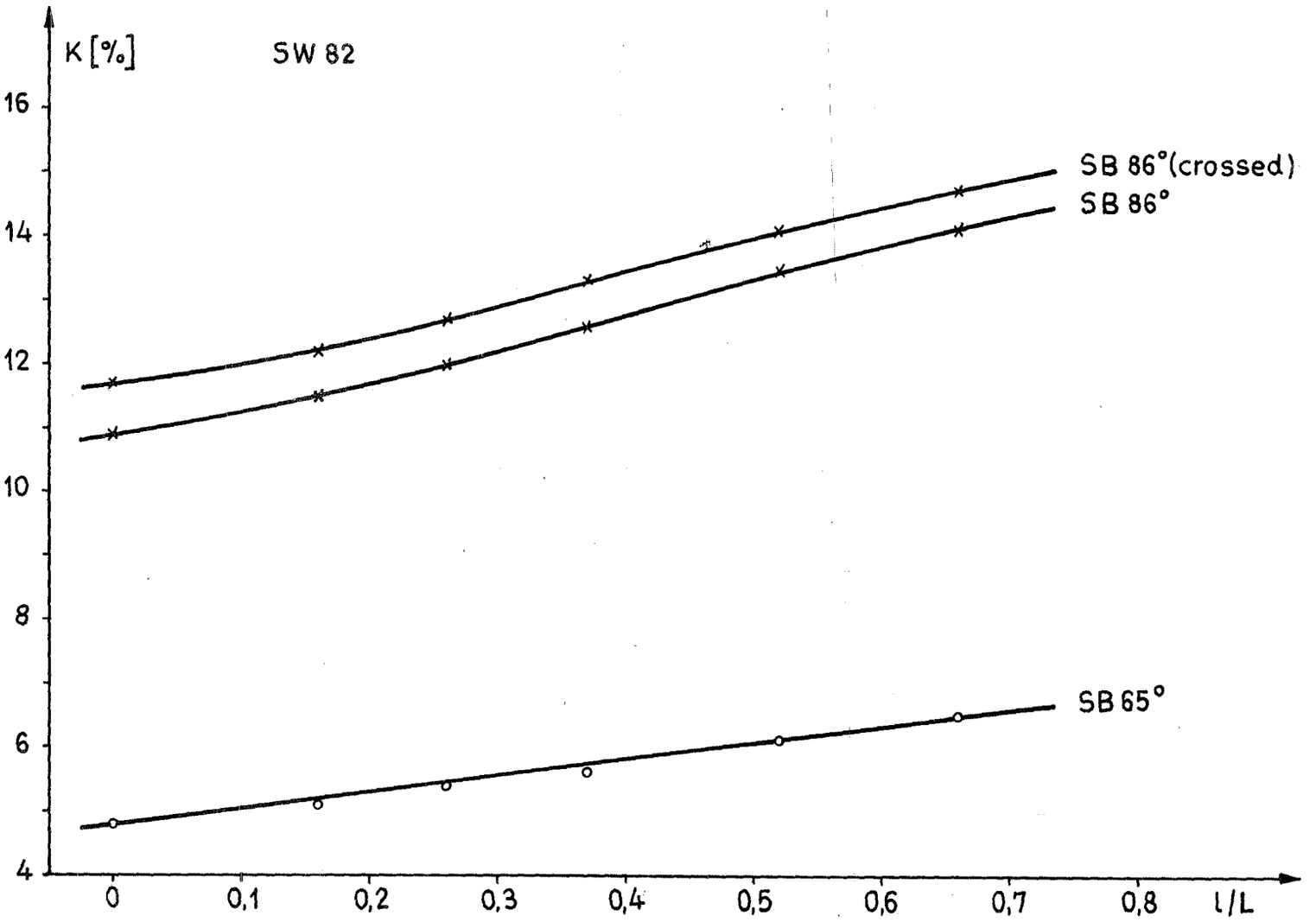
K [%]
SW 82
16
14
12
10
8
6
4
SB 86°(crossed)
SB 86°
SB 65°
0
0,1
0,2
0,3
0,4
0,5
0,6
0,7
0,8
l/L

Fig. 27

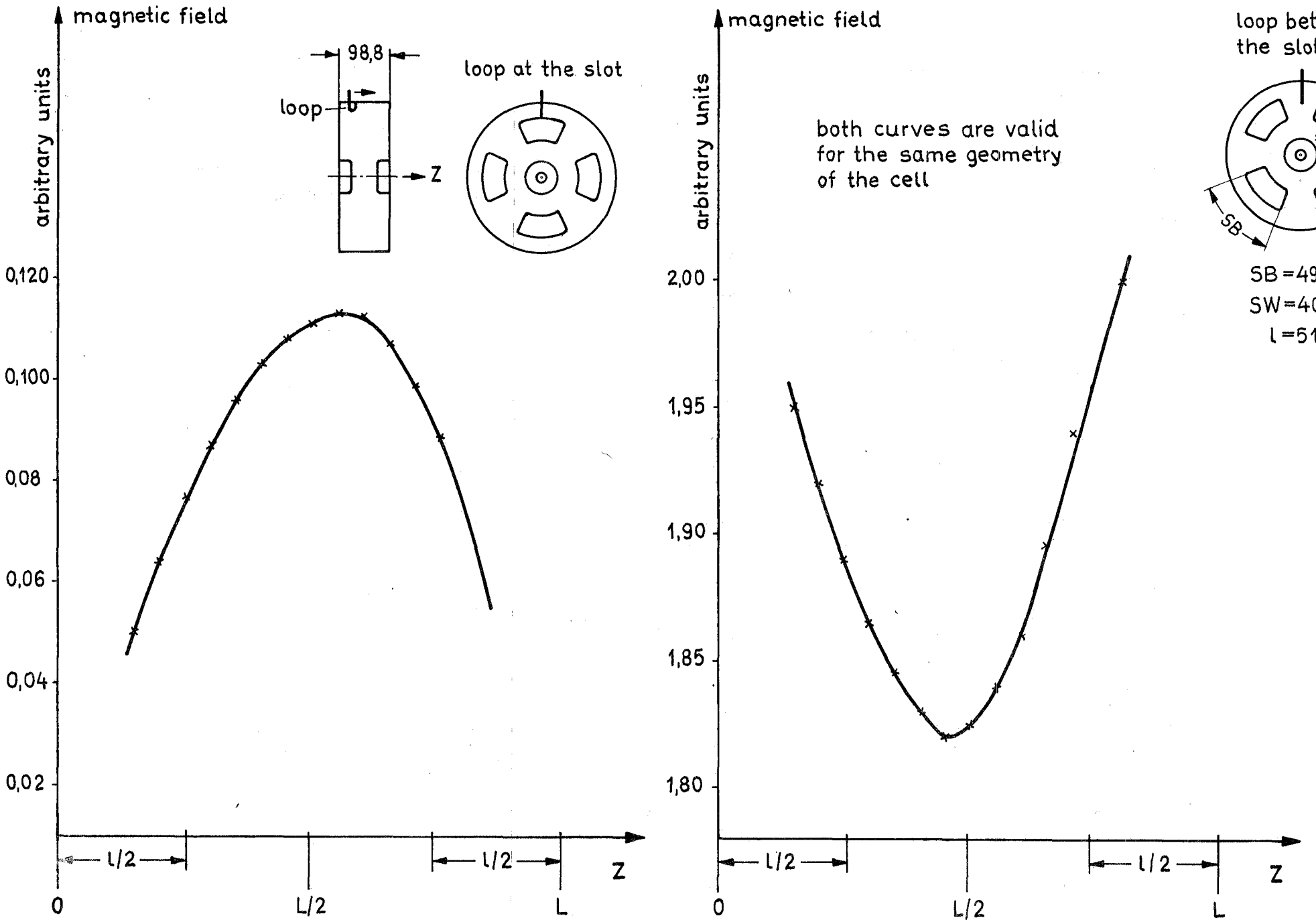
magnetic field
arbitrary units
98,8
loop
b
z
loop at the slot
0,120
0,100
0,08
0,06
0,04
0,02
l/2
l/2
z
0
L/2
L
magnetic field
arbitrary units
both curves are valid
for the same geometry
of the cell
loop between
the slots
SW
SB
SB=49°
SW=40mm
l=51mm
2,00
1,95
1,90
1,85
1,80
l/2
l/2
z
0
L/2
L

Fig. 30